Ann. Univ. Stell. Ser. A1 (Geol.) Vol. 3 p. 1-66, 1981

ICE SHEET DEFORMATION IN THE TABLE MOUNTAIN GROUP, WESTERN CAPE

by

H. J. BLIGNAULT

Revised version of thesis presented for the degree of Master of Science at the University of Stellenbosch

May, 1970

ABSTRACT

The Lower Paleozoic glaciogenic sediments of the Table Mountain Group are interpreted as the result of two ice sheet advances into the active Table Mountain embayment. Subglacial deformation during the first advance gave rise to the Fold Zone. Macro- and micro-fabric data of deformed and undeformed sediments provide valuable constraints on the interpretation of the rheology of sediment transport media and the contemporaneously deformed sediments.

It is shown that the structural characteristics of the Fold Zone are consistent with the progressive infill of the Table Mountain embayment by an ice sheet. The distribution, size and geometry of the folds are dependent on the effective load of the ice sheet and the type and direction of ice sheet flow; compressive and extending flow resulted in pure shear and simple shear deformation respectively.

SAMEVATTING

Die glasiogene sedimente van die Onder-Paleosoïese Tafelberggroep word verklaar as die sedimentasie-produk van twee ysplaatbewegings in die aktiewe Tafelberginham. Die Plooisone word geassosieer met onderysplaatdeformasie tydens die eerste ysplaatbeweging. Die rheologie van die sedimentasietransportmedia en die gedeformeerde sedimente van die Plooisone is ondersoek deur gebruik te maak van maakselanalises.

'n Model is opgestel waarvolgens die struktuur van die Plooisone ooreenstem met die progressiewe opvulling van die Tafelberginham deur 'n ysplaat. Hiervolgens is die verspreiding, grootte en geometrie van die plooie 'n funksie van die effektiewe ysplaatbelading en tipe en rigting van ysplaatvloei; kompressiewe en verlengingsvloei het oorlangse en eenvoudige skuifskeurvervorming respektiewelik veroorsaak.

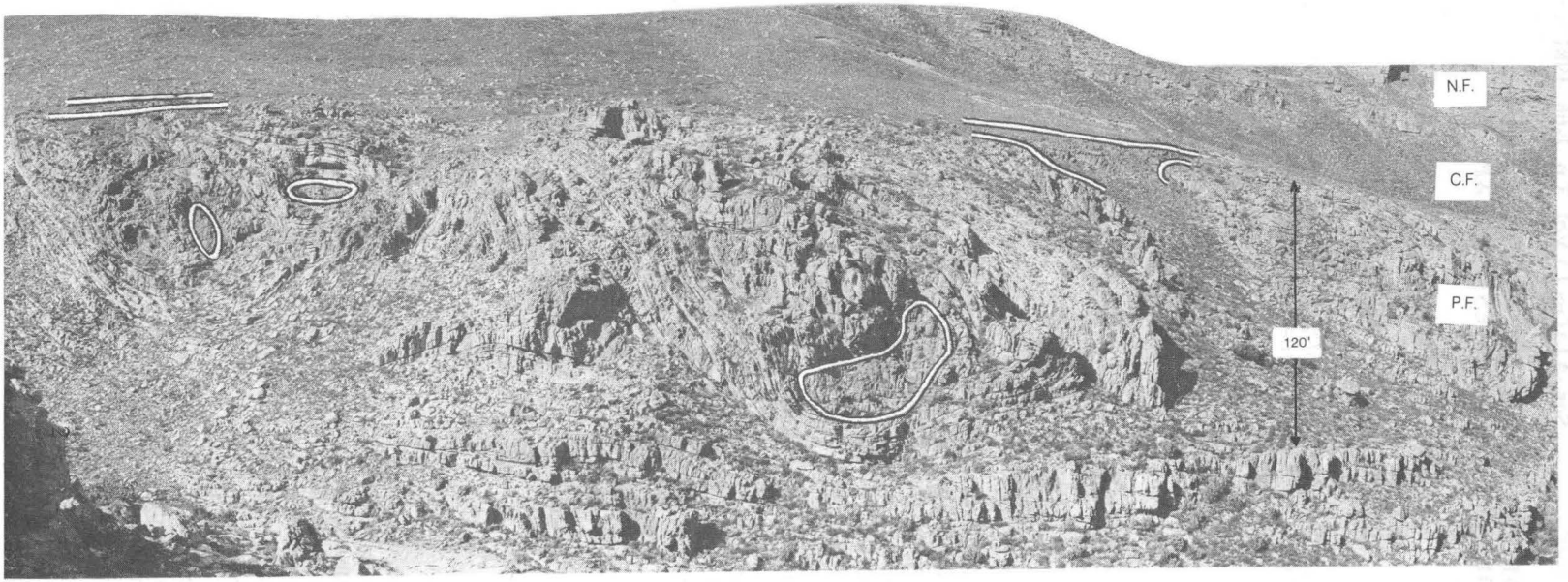

NARDOUW FORMATION – N.F.
CEDARBERG FORMATION – C.F.
PAKHUIS FORMATION – outlined
PENINSULA FORMATION – P.F.

PLATE I
The Fold Zone at De Bailie.

CONTENTS

1. INTRODUCTION

1.1 STATEMENT OF PROBLEM

A zone of intraformational folding within the paleozoic Table Mountain Group is widespread throughout the Western Cape Province. The contemporaneous nature of the deformation is well established by its stratigraphic setting. It constitutes a distinctive stratigraphic unit of unusual width. A glacial mode of origin for the folding and some of the associated sediments has been widely accepted, but various opinions have been expressed about the detailed relationships and probable sequence of events.

The object of this study was

(i) to document the internal and external geometry of the Fold Zone,
(ii) to determine the relation between the intraformational folds and the overlying Pakhuis diamictites and
(iii) to construct an hypothesis regarding the mode of deformation.

1.2 METHODS

1.2.1 *Selection of areas*

Ideal localities for field investigation are limited by the north-south trending tectonic folds of the Cape Fold Belt which control the development of a rugged mountainous landscape. The areas selected for fieldwork (Fig. 1) are located on the broad, subhorizontal hinge zone of the Cedarberg anticline, its wavelength being of the order of tens of kilometres. The culmination point is situated at Sneeukop (Eselbank) from where the axis plunges gently north and south.

1.2.2 *Mapping*

As a first approach, an area 2 000 ft × 4 000 ft (600 m × 1 200 m) at De Trap (Map 1) was mapped by plane table and telescopic alidade. The regional stratification attains a maximum dip of 10° towards the south-east. For orientation studies the regional attitude was assumed to be horizontal as direct field measurement was not always possible.

The variability of the fold elements was subsequently determined on a regional basis and maps (Figs. 13, 14 & 32; cf. locality map, Fig. 1) were compiled from uncontrolled mosaics. Orientation data are corrected where tectonic tilt exceeds 5°.

1.2.3 *Stereographic analysis*

All three-dimensional orientation data were compiled in the lower hemisphere of an equal-area Schmidt net as described by Turner and Weiss (1963), using the grid method for contouring.

1.2.4 *Primary macrofabric analysis*

The preferred orientation of clasts in the Pakhuis diamictites was determined at De Trap, using Member divisions to define sampled populations. The number of measurements depended on the availability of suitable clasts in every Member. The sample domain is shown by the outcrop distribution of the Members (Map 1). The lower Sneeukop Member was subsampled by defining each synclinal core as a separate population.

By introducing a controlled bias, any inherent preferred orientation should be accentuated. This was accomplished by using well developed rod-like and discoidally shaped clasts to measure the attitude of A and the A$\underline{B}$-surface respectively. The long axes of rod-like clasts varied from 2 to 28 cm; care was taken to ensure that the A/$\underline{B}$-ratio exceeded 1,5. The majority of clasts were discoids.

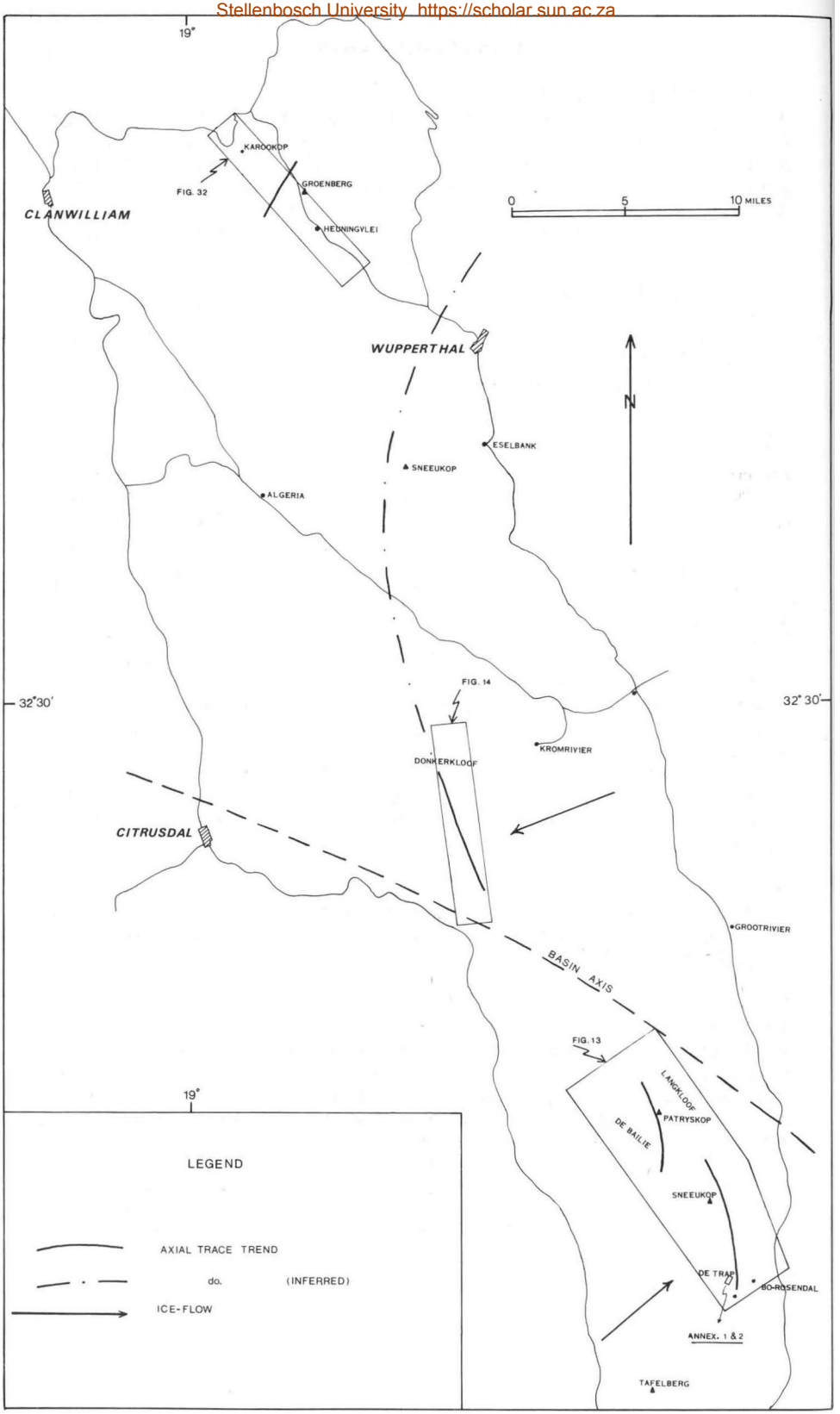

Fig. 1. Locality map and regional configuration of Fold Zone structures.

1.2.5 *Microfabric analysis*

The preferred orientation of the long axes of quartz grains was determined both for primary and deformed fabrics. Surfaces of maximum fabric contrast, defined by the preferred orientation of A′ on any boundary surface of a layer, were investigated with a stereomicroscope, using either reflected or polarized light for best definition of grain boundaries. A circle-segmented graticule, fitted in the objective, was used for rapid grouping of orientations in 20° classes (modulo π).

Only grains with an A′/B′ -ratio exceeding 1,5 were used. By subsampling on a differential grain size basis, an attempt was made to determine whether orientation is a function of grain size. Separate counts were made of fractions with A′ smaller than 0,4 mm and larger than 1,0 mm. Grains larger than 1,0 mm in diameter were too few to warrant further subsampling on the available slabs. The number of grain counts (n) was determined by subsequent sampling; 100-150 counts usually sufficed.

Compass diagrams (co. dgms., see Blignault 1970) were compiled from these data and used to infer modal vectors. The central position of a modal class or classes constituting a mode was used to define the statistical orientation of A′. Block diagrams (Figs. 5, 7, 10, 25, 26, 28), depicting only the modal vectors, illustrate the three-dimensional fabric pattern. Arrows on block diagrams indicate primary modal vectors while broken arrows represent secondary modal vectors and hatched circles show a random distribution; the azimuthal notations with five digits refer to true north with the last two digits indicating the dip towards the right hand side when looking towards the strike direction; the zero position of the orientation circle on the main bounding surface is referred to true north either by a strike or dip direction or by the projection there-on of true north; where the direction of a (Sed.) is indicated it has been corrected for tilt where necessary. All sample localities are indicated on Map 2.

The interpretation of primary directional properties from the three-dimensional fabric patterns is based on the assumption that the fabric pattern on the bc (Sed.) -surface is either a random distribution and/or defines a monoclinic symmetry with the ac-surface as the symmetry surface.

No significant experimental errors have been introduced during the preparation of orientated polished sections or slides. Determination of the depositional surface, however, is problematic. The attitude of intercalated arenite lentils in the lower Sneeukop Member indicates the orientation of ab (Sed.) for samples taken nearby. For the upper Sneeukop Member and Steenbras Member (De Trap) ab (Sed.) is assumed to be subhorizontal i.e. a maximum dip error of 10° is introduced. Where this direction of dip is subparallel to the preferred orientation A′ on ab (Sed.) and the imbrication angle is 10° or less, erroneously inferred transport directions may result.

1.2.6 *Radiography*

Rock slabs measuring approximately 4 cm × 5 cm × 0,3 cm were cut parallel to ac (Sed.) of the Pakhuis diamictites and submitted to Dr. I. O. Faiman, Cape Town, for radiography. Technical details are:

film:	Cronex X-ray
exposure:	25 ma × 3 seconds
KV:	40
distance source-film:	100 cm
developing time:	3 minutes

The radiographs revealed no internal structures in the rock.

1.2.7 *Terminology and notations*

The terms used to describe folds are those proposed by Fleuty (1964) and the terminology for layering has been defined by Elliot (1965).

A, B & C	Long, intermediate and short axes of clasts.
A′	Apparent long axes of clasts.
a, b & c (Sed.)	Orthogonal reference system for primary directional properties of sediments (Potter and Pettijohn, 1963) ab – principal surface of deposition a – line of movement b – sedimentary strike
a′, b′ & c′ (Sed.)	Reference system for deformed sedimentary fabrics.
a, b & c (Geom.)	Orthogonal reference system which denotes the monoclinic fabric of a tectonite geometrically (Whitten, 1966). ab – most prominent foliation ac – monoclinic plane of symmetry b – normal to the monoclinic plane of symmetry, parallel to B, the fold axis.
a, b & c (Kin.)	Orthogonal reference system which denotes the kinematic axes of a monoclinic tectonite fabric (Whitten, 1966). a – line of movement b = B – axis of external rotation ac – plane of deformation ab – slip surface
S_1	Surfaces bounding cross-laminae.
S_2	Stratification surfaces ("bedding planes").
S_3	Surfaces bounding tansposed/rotated cross-laminae (transposed bands will be referred to as S_3-bands).
S_4	Surfaces bounding a set of S_3-bands (a set of S_3-bands will be referred to as S_4-bands).
L_1	Intersection between S_1 and S_2.
L_2	A special type of lineation, cf. section 2.2.3.2 (ii) b.
B	Fold axis
β'	Zone axis

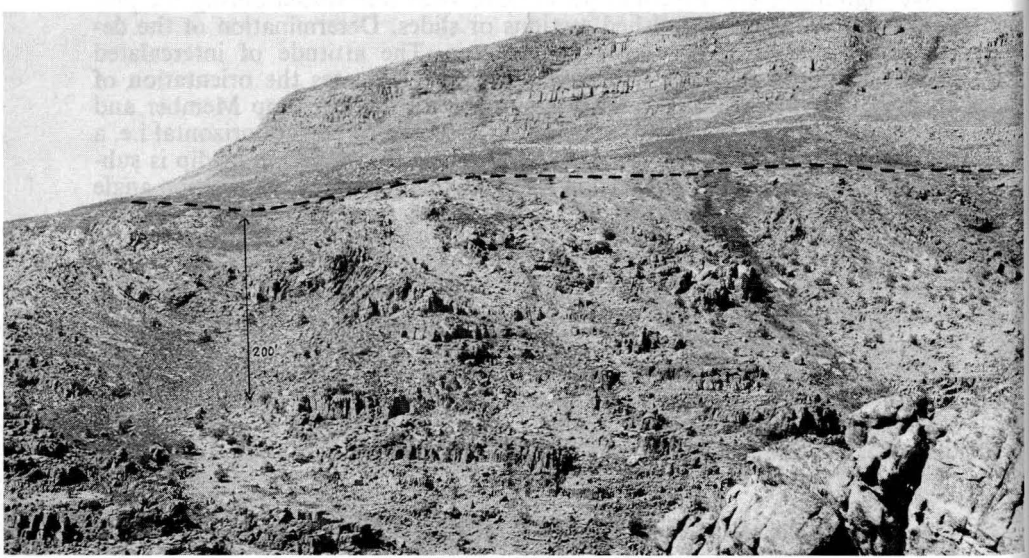

PLATE II

Upright folding at Langkloof; note the broad synclines and narrow, cuspate anticlines. The upper boundary of the Fold Zone constitutes a structural discontinuity.

1.3 LITERATURE REVIEW

The intraformational folding was first described by Haughton et al., 1925. They concluded that the folds formed transversely to the direction of ice-flow in front of the contact line between an ice mass and the underlying sand. An easterly direction of ice-flow was inferred from the fold asymmetry. "The horizontality of the main band of tillite . . . above . . ." the folding led them to the view that the tillite was subaqeously deposited.

Haughton (1929) reported intraformational folding in both the Peninsula and Nardouw Formations of the Table Mountain Group, which was taken as evidence for more than one glacial advance.

Visser (1962) regarded the tillite as a terrestrial glacier deposit; deposition took place after the advance of individual glaciers along synclinal valleys. Ice-flow was parallel to the fold axes from the north-northeast, as inferred from two petrofabric analyses as well as heavy mineral distribution and so-called glacial floors.

Rust (1967), during the course of a regional survey, compiled extensive data pertaining to the orientation of the fold axes (cf. his Fig. 99). He concluded that an ice-sheet advanced from north to south, parallel to the regional trend of the fold axes; the ice effected huge loadcasts which became elongated in canoe-shaped folds due to the forward motion of the ice sheet. The Sneeukop tillite represented an englacial deposit in the pod folds. Paleo-iceflow was determined by petrofabric analysis on 13 samples from the Pakhuis tillites and 9 "glacial floors".

1.4 PRESENT INVESTIGATION

The field-work for this study was completed in 1969. As a result of the long delay before publication, the sections dealing with geological structure and the final interpretation were extensively revised and rewritten by the author in June 1979. It was found impractical to convert all heights and distances on the text figures to the metric system which is now used in South Africa (1 ft = 0,3048 metre, 1 mile = 1,609 kilometres).

2. OBSERVATIONAL DATA

2.1 LITHOLOGY OF STRATIGRAPHIC SEQUENCE

2.1.1 *Stratigraphy*

The lithostratigraphic sequence of the Table Mountain Group, as established by Rust (1967), is presented in Table 1 and used in this text.

Brachiopods from the Cedarberg Formation indicate an upper Ordovician (Ashgill) age (Cocks et al., 1969). Rust consequently estimates that the Table Mountain Group sedimentation spans the entire Ordovician and Silurian Periods.

Penecontemporaneous deformation enables the establishment of an informal time-stratigraphic sequence. The value of each time marker is dependent on the duration of the deformational event. Stages and substages can be delimited within such an undefined series (cf. Table 2). Stage B, which is delimited by the first deformational phase and the Brachiopod Zone, is further subdivided by a second period of deformation into Substages B-1 and B-2. The boundaries of these time-stratigraphic sequences parallel the member and formation subdivisions on a regional scale in the western Cape.

2.1.2 *Peninsula formation*

The lithology of the Peninsula Formation has an important bearing on the penecontemporaneous deformation in its uppermost horizon. The most important characteristic is its lithologic homogeneity. Stratification is invariably cross-laminated (planar type) and varies in thickness from 2 ft. to 10 ft. (0,6 m-3 m); the cross-laminae vary in thickness from 1 to 8 cm.

TABLE 1

THE STRATIGRAPHY OF THE TABLE MOUNTAIN GROUP AFTER RUST (1967)

	Formation	Member	Maximum thickness
TABLE MOUNTAIN GROUP	Nardouw	sandstone	3,000 ft (915 m)
	Cedarberg	Disa Siltstone Soom Shale	450 ft (140 m)
	Pakhuis	Kobe Tillite Steenbras Tillite Oskop Sandstone Sneeukop Tillite	400 ft (120 m)
	Peninsula	sandstone	6,000 ft (1 830 m)
	Graafwater	purple fine sandstone	1,400 ft (430 m)
	Piekenier	conglomeratic ss.	3,000 ft (915 m)

Microscopic observations show that:

(i) The formation consists essentially of a medium grained (mode approximately 0,6 mm) quartz arenite.
(ii) The arenite is well sorted; no matrix is present.
(iii) The sand is cemented by overgrowth quartz, the detrital cores being suspiciously well rounded.
(iv) The detrital cores are partly afloat in the cement, indicating a loose packing. Where the framework is intact most contacts are tangential.
(v) No dynamic metamorphic effects were detected at De Trap and De Bailie. This generally applies to the entire Formation in the Cedarberg area.

2.1.3 *Fold Zone*

The uppermost portion of the Peninsula lithosome and the overlying lower Sneeukop Member were folded prior to the deposition of the superposed sediments, and constitute the Fold Zone. The penecontemporaneous aspect of the folding is reflected by the environmental associations between the lower Sneeukop Member and the rest of the Pakhuis Formation.

The folding dies out downwards and locally forms a regular décollement surface (Plate I). The overlying sediments are unconformably related to the Fold Zone; the contact surface is regular and erosional features are evident from structural discontinuities (Plate II).

The areal distribution and external geometry of the Fold Zone in relation to the embayment axis (it is assumed that the geometry of the basin is related to the geometry of the basin fill) are shown in Fig. 2; a genetic association is implied by the symmetric relationship. The Fold Zone attains a maximum thickness of 300 ft (90 m).

Profiles of the Fold Zone (Fig. 3) illustrate the following conspicuous features:

(i) The presence of isolated centres of no deformation.
(ii) Both abrupt and gradual decrease in Fold Zone thickness towards the isolated centres of no deformation.
(iii) Regional fluctuations of Fold Zone thickness.

TABLE 2

AN INFORMAL TIME-STRATIGRAPHIC SUBDIVISION OF THE TABLE MOUNTAIN GROUP

TABLE MOUNTAIN GROUP	Litho-stratigraphic unit		Time-stratigraphic unit		Boundaries of time-stratigraphic units
	Formation	Member	Stage	Substage	
	Cedarberg	Disa	C (post-glacial)		Brachiopod Zone (Ashgill)
		Soom	B (glacial)	B-2	
	Pakhuis	Kobe			
		Steenbras			2nd Period of Deformation
		Oskop		B-1	
		Upper Sneeukop			1st Period of Deformation
		Lower Sneeukop	A (glacial)		
	Peninsula		A (pre-glacial)		

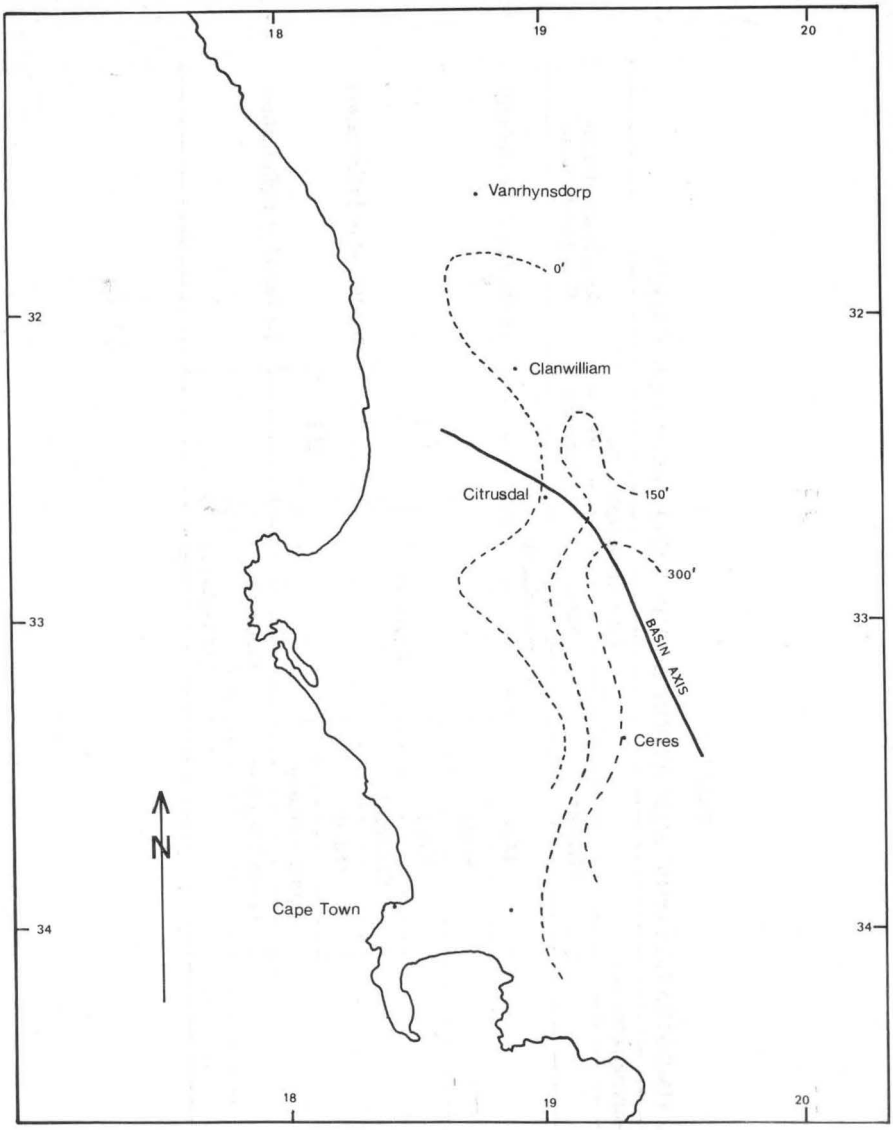

Fig. 2. External geometry of the Fold Zone.
The broken lines show the variation in Fold Zone thickness in relation to the embayment axis; compiled from Rust, 1967 (Figs. 99 and 112).

Fig. 32 illustrates the marginal character of the Fold Zone which in section would appear like a thin (0 m-3 m) discontinuous, tapering zone with sparsely distributed belts of deeper (4 m-12 m) deformation (cf. Fig. 32; Karookop).

Microscopic comparisons between the deformed and undeformed quartz arenite of the Peninsula Formation reveal no compositional and textural differences. Structurally, though, there is a significant difference; the folded S_4-banding (the apparent stratification) is conspiciously thinner (60 cm) than the undeformed cross-stratified layers immediately below the Fold Zone.

The sympathetically folded lower Sneeukop Member is described in Section 2.1.4.2

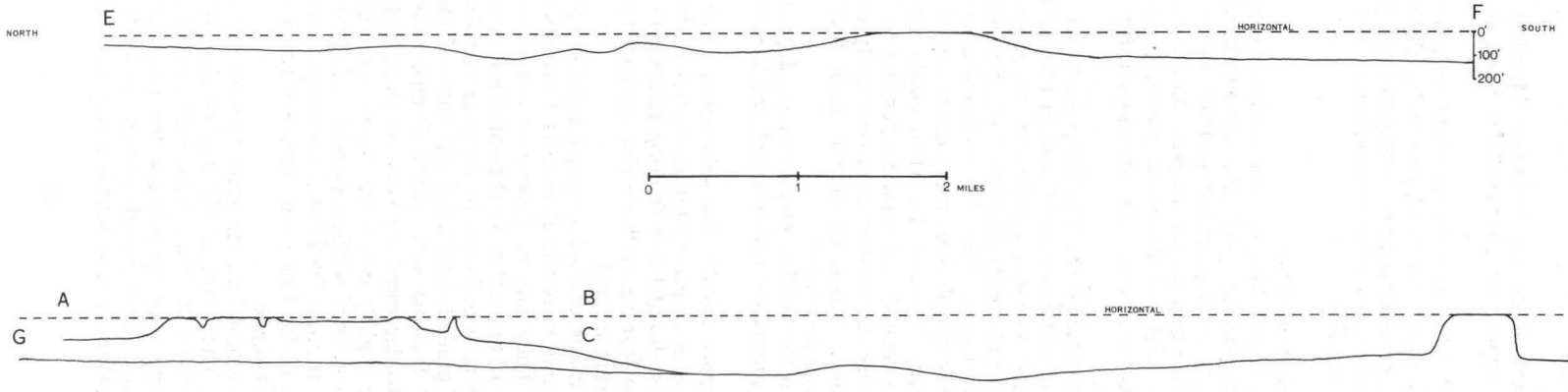

Fig. 3. Profiles of the Fold Zone.
The lower limit of the Fold Zone is shown relative to the horizontal which represents the upper boundary. The section lines are shown on Figs. 13 and 14.

2.1.4 *Pakhuis formation*

2.1.4.1 Introduction

For the sake of convenience the Sneeukop Member is informally divided into a lower and an upper part, the boundary being the upper surface of the Fold Zone.

The Kobe Tillite Member should be grouped with the Cedarberg Formation because (i) lithostratigraphic principles (A C S N, 1961) demand lithologically alike sediments to be grouped together irrespective of genetic considerations; and (ii) the Kobe Member is a facies variation of the Soom Shale Member of the Cedarberg Formation.

2.1.4.2 Lower Sneeukop member

The lower Sneeukop Tillite Member constitutes the upper part of the Fold Zone. It typically occupies the synclinal cores which, in some instances, have become isolated due to tight overfolding (Plate I and Map 1). Originally it was probably a blanket deposit not thicker than 6 m-12 m.

The lower contact with the Peninsula arenite is usually sharp and conformable but irregular structure is also developed. Fig. 4A illustrates an unconformable contact.

Some megaclasts typical of the Sneeukop diamictite are partly embedded in the upper bounding surface of the Peninsula Formation.

The lower Sneeukop Member consists of arenaceous diamictite (Flint et al., 1960 a, 1960 b) which rarely displays "stratification". No internal structures are revealed by radiographs. The rudite fraction of the diamictite is sparsely and randomly distributed; these clasts are of variable composition but consist dominantly of quartzite. Most clasts are waterworn discoids, commonly faceted, polished and striated parallel to their AB-planes. The following features were determined microscopically on the diamictite:

(i) The arenite grains consist of quartz, rock fragments and accessory zircon, tourmaline and rutile.
(ii) The mode within the arenite fraction ranges from 0,3 mm to 0,6 mm.
(iii) The arenaceous grains are well rounded and loosely packed with tangential contacts.
(iv) The interpore space (5-10% by volume) is filled by smaller particles floating in a mass of cryptocrystalline material which represents the diagenetically recrystallized lutite fraction (authigenic sericite, biotite and pressure solution features indicate that at least the anadiagenetic stage was reached during burial).

Lenticular bodies of a fine grained arenite (modal development in the 0,2-0,3 mm range) were found near the Peninsula Formation/Sneeukop Member contact (cf. Map 1). They vary in thickness from 60 cm to 150 cm and continue along strike for 12 m to 30 m. In the only thin section prepared the lower contact with diamictite was found to be microscopically sharp. Internally the lenses consist of graded, laminated (0,1 mm-0,5 mm) sets (5 cm-10 cm) which show normal faulting with slight displacement, penetrative within 5 mm-15 mm. The displacement surfaces are sharply defined. Some laminae have sagged and are slightly contorted. These structures are interpreted as collapse structures associated with ice-contact sediment (see Boulton, 1972).

Fig. 4B depicts what could be a fossil ice-wedge or esker at De Trap. The contact between the wedge-like small-pebble diamictite body and the surrounding diamictite is vague.

Medium to coarse grained quartz arenite lentils are sporadically interbedded in the diamictite. The lentils usually are less than 60 cm thick and have a strike-length of 1,5 m-12 m. They have well-defined convex-shaped lower boundaries which were used to indicate the geopetal relation (Plate III). The orientation of these lentils largely proves the folded nature of the lower Sneeukop Member (Map 1). The lentils rarely have an intertonguing rela-

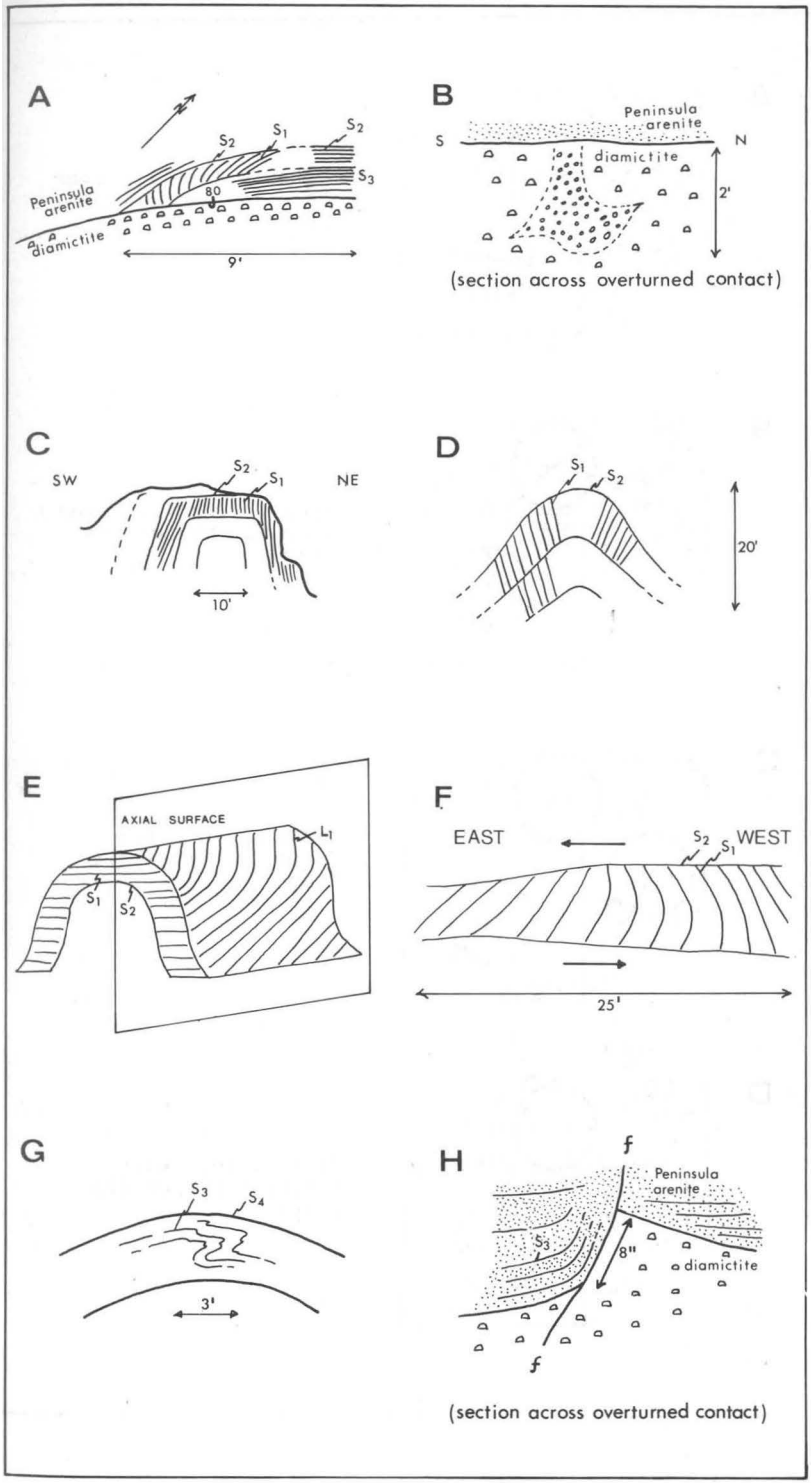

Fig. 4. Deformational features of the Fold Zone; see text for explanation.

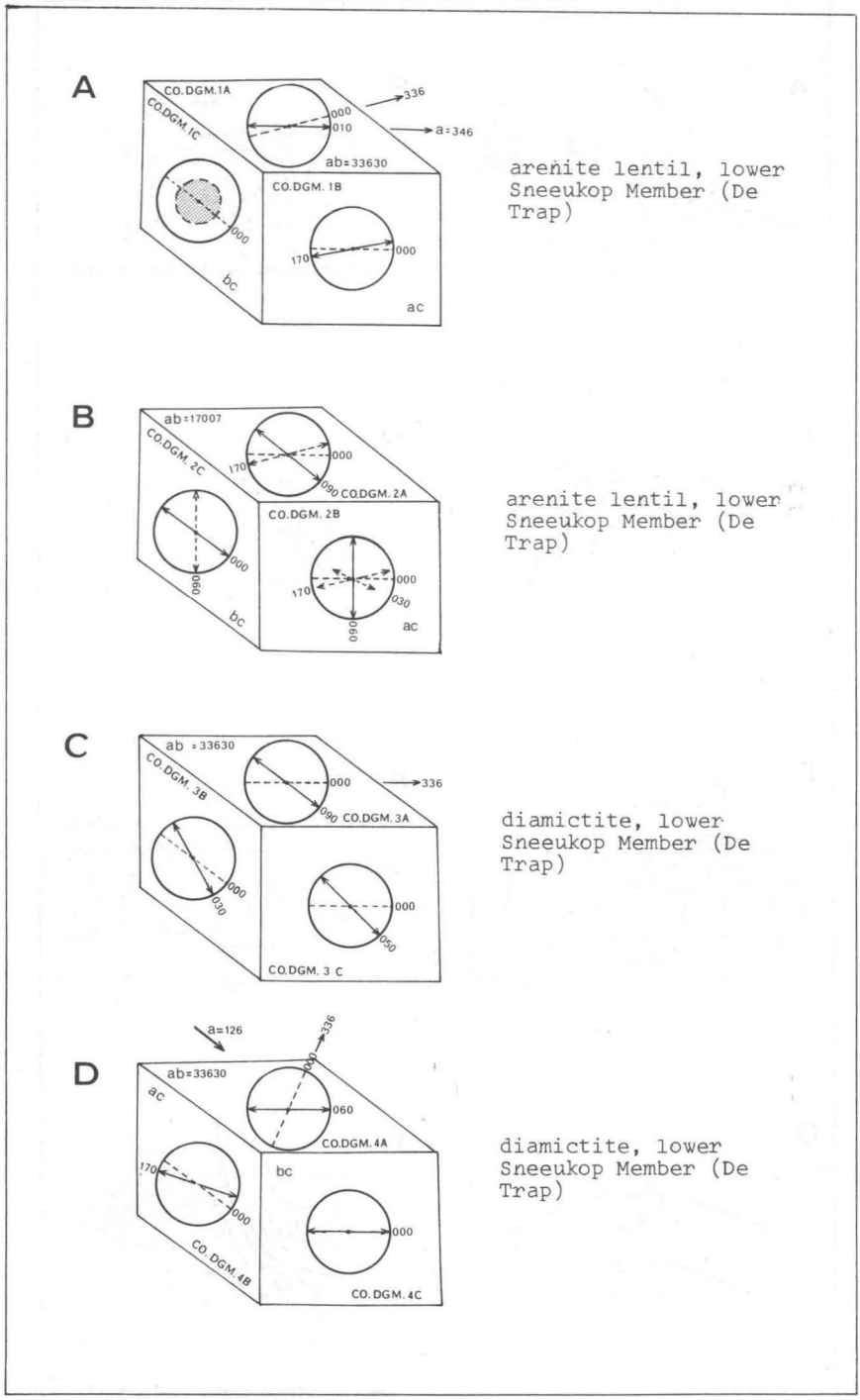

Fig. 5. Three-dimensional microfabric patterns as defined by the preferred orientation of quartz grain long axes. Sample localities 5A to 5D are shown on Map 2.

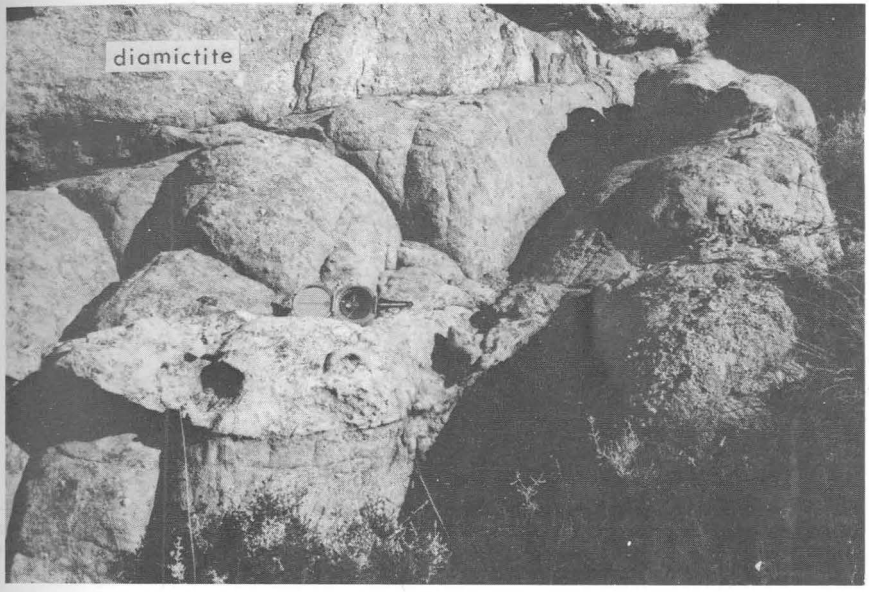

PLATE III
An arenite lentil within the lower Sneeukop Member (De Trap).

tionship with the surrounding diamictite. The contacts commonly are graded. Microfabric analyses of two lentils indicate flow in a direction 346° (Fig. 5A) and parallel to 170° (Fig. 5B, Map 2) (the localities with the vectorial data are shown on Map 2 by the Figure number). The two three-dimensional fabric patterns suggest altogether different modes of transport; Fig. 5A, a typical example of an uncomplicated fabric pattern, depicts longitudinal transport with a low negative imbrication angle, probably typical of lamellar flow. More turbulent fluid-flow conditions are inferred from the complex pattern shown in Fig. 5B:

(i) Imbrication angles are large and variable, indicating a rotational movement around b (Sed.).
(ii) The two principal modes on the ab (Sed.)-plane, with a non-orthogonal relation, are evidence of a longitudinal as well as a transverse mode of transport; the grains transported in a longitudinal fashion, typical of suspended particles, had less constraint exercised upon them (therefore the non-orthogonal relationship) than those transported transversely i.e. by traction.

It is possible that these fabric patterns were altered somewhat by the subsequent glacial folding; the simple primary microfabric pattern of Fig. 5A, however, shows that the deformation was not penetrative.

The macrofabric pattern of diamictite exposed in two separate synclinal cores, was determined using discoidally shaped clasts (Figs. 6A & B). The preferred imbrication of the discoids suggests 'flow' towards a south-easterly direction. The 'flow' direction is considered an apparent flow direction because

(i) the assumption that the depositional interface is subhorizontal across the area sampled (synclinal cores of diamictite), is erroneous and
(ii) it is possible that the clasts were rotated during the folding process i.e. the present fabric is the result of a deformational fabric superposed on

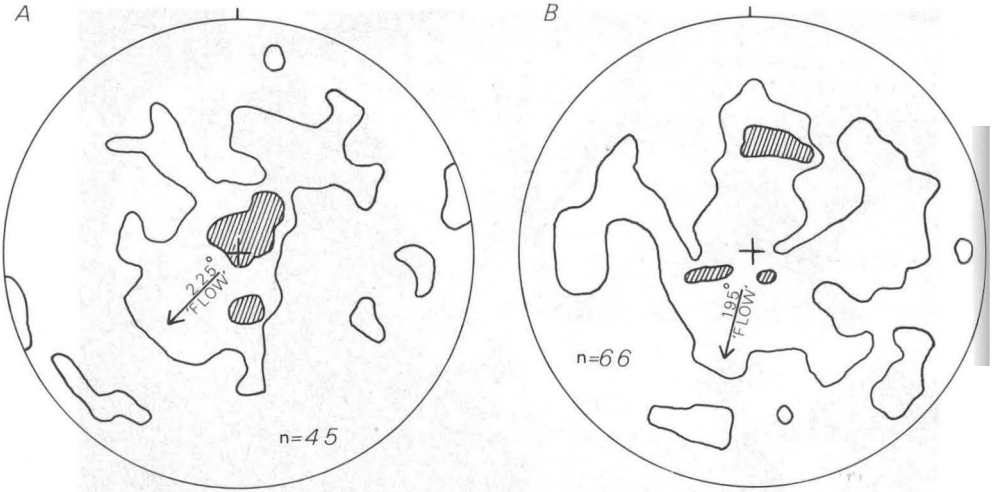

Fig. 6A and B. The preferred orientation of maximum dip lines (with respect to the horizontal) of discoidal clasts at two sample stations in the lower Sneeukop Member. Contours indicate total distribution and >6% points per 1% area. Sample localities are shown on Map 2. The 'flow' direction is apparent and not directly related to primary flow.

a primary fabric (cf. the primary macrofabric pattern of the upper Sneeukop Member, Fig. 9A, with Fig. 6).

Figs. 5C & D, 7A & B illustrate the three-dimensional microfabric patterns established for four samples from the lower Sneeukop diamictite. The vectorial data of 5D and 7A are compiled on Map 2. Although the size differentiated analysis does not prove different modes of transport for different size fractions, it is evident that the transport medium exerted more constraint on the orientation of the larger sized particles (cf. Fig. 8). It may still be possible to prove orientation as a function of size by increasing the gap between the two size fractions. Different modes of transport have been established for different samples; the grains with longitudinal modes of transport have high (50°) or variable angles of imbrication (Figs. 7A & B) while a larger constraint in the ac(Sed.)-plane and a low angle (10°) of imbrication is evident for transverse transport (Fig. 5D). The non-orthogonal bimodal pattern on the ab(Sed.)-plane of one sample (Fig. 7A) is significant in that it appears to represent critical fluid-flow conditions between that necessary for transverse (Fig. 5D), and longitudinal (Fig. 7B) modes of transport. Three samples may thus represent fabric patterns reflecting three different flow regimes. Two samples taken within 3 m of one another (30 cm vertically) have different fabric patterns (Figs. 5C & D), perhaps suggesting short distance variability in the flow regime. The one sample, measuring 7 cm × 5 cm × 3 cm, does not even constitute a homogeneous domain (Fig. 5C); the modes on the vertical planes do not define the mode on the ab(Sed.)-plane. This heterogeneity and apparent different transport modes can be ascribed to either

(i) variability in the flow regime, or
(ii) later deformation.

2.1.4.3 Upper Sneeukop Member

The upper Sneeukop Member overlies the Fold Zone unconformably. This unconformity commonly is an undulating surface with the low areas related to underlying synclines. The upper Sneeukop Member is a blanket

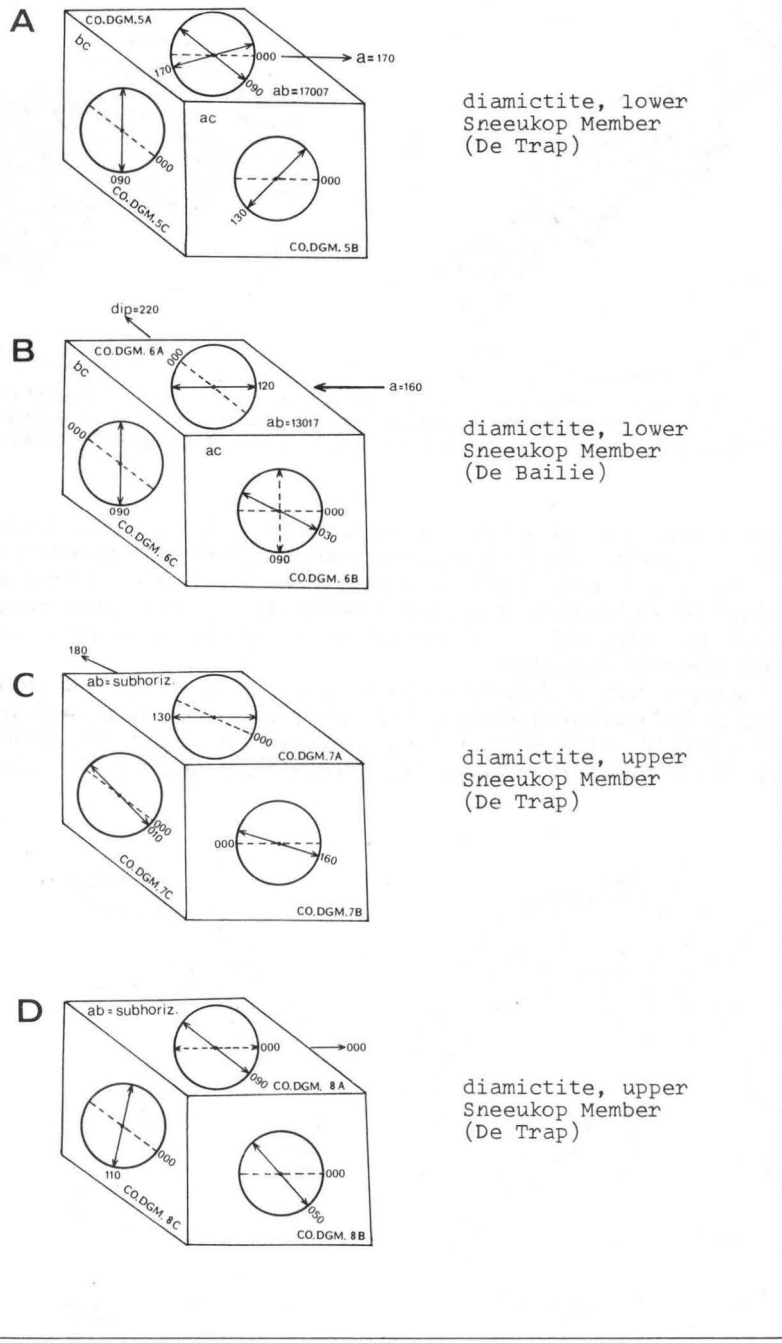

Fig. 7. Three-dimensional microfabric patterns as defined by the preferred orientation of quartz grain long axes. Sample localities 7A to 7D are shown on Map 2.

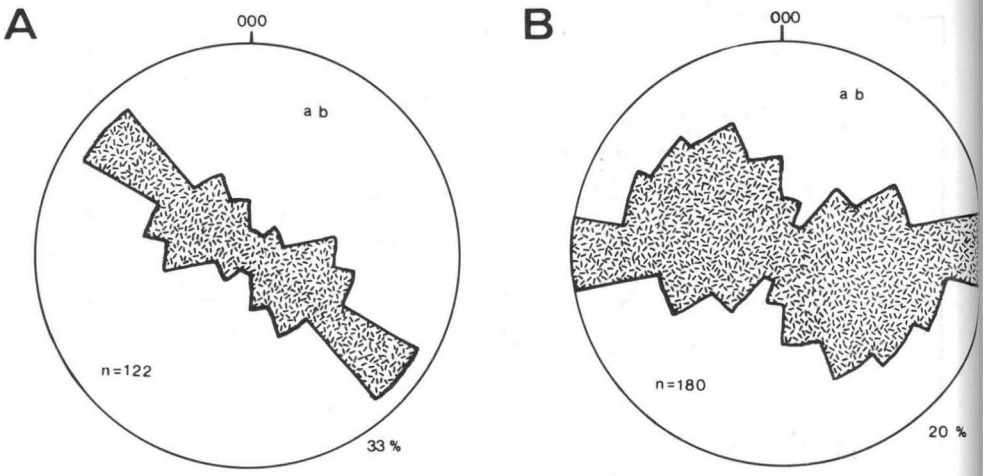

Fig. 8. The preferred orientation of quartz grain long axes on the depositional interface (ab). See Fig. 7B for the three-dimensional microfabric pattern of the same sample (lower Sneeukop Member, De Bailie). A. Long axes $\geq$ 1 mm. B. Long axes $\leq$ 0,4 mm.

deposit, estimated not to exceed 12 m in thickness. It consists dominantly of feebly "stratified" (30 cm-60 cm) arenaceous diamictite; no internal structures were revealed by radiography. Thin (less than 15 cm) beds of quartz arenite and pebble washes occur frequently towards the top. The upper arenaceous diamictite corresponds in all textural and compositional features with the lower Sneeukop diamictite.

The fabric pattern of the rudite fraction, representative of the mapped area (Map 2), defines flow in direction 172°. The preferred imbrication of discoids and rods (Figs. 9A & B) from the same sampled area, indicates a southerly flow of the transport medium. The uncertain dip factor ($\pm$10°) does not

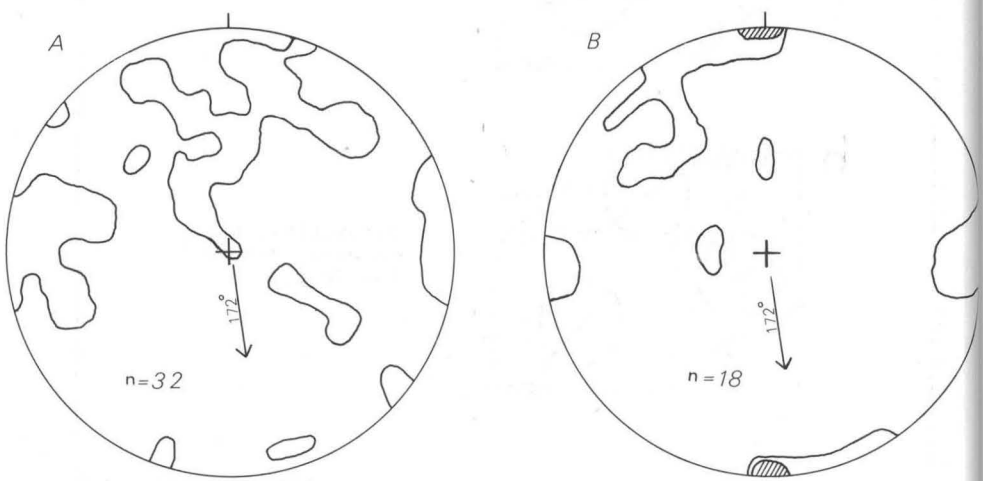

Fig. 9. Macrofabric patterns of the upper Sneeukop Member. A. The preferred imbrication of maximum dip lines of discoidal clasts indicates a southerly flow. Contours show total distribution. B. The preferred inclination of rod-shaped clasts suggests a southerly flow. Contours show total distribution and >20% points per 1% area.

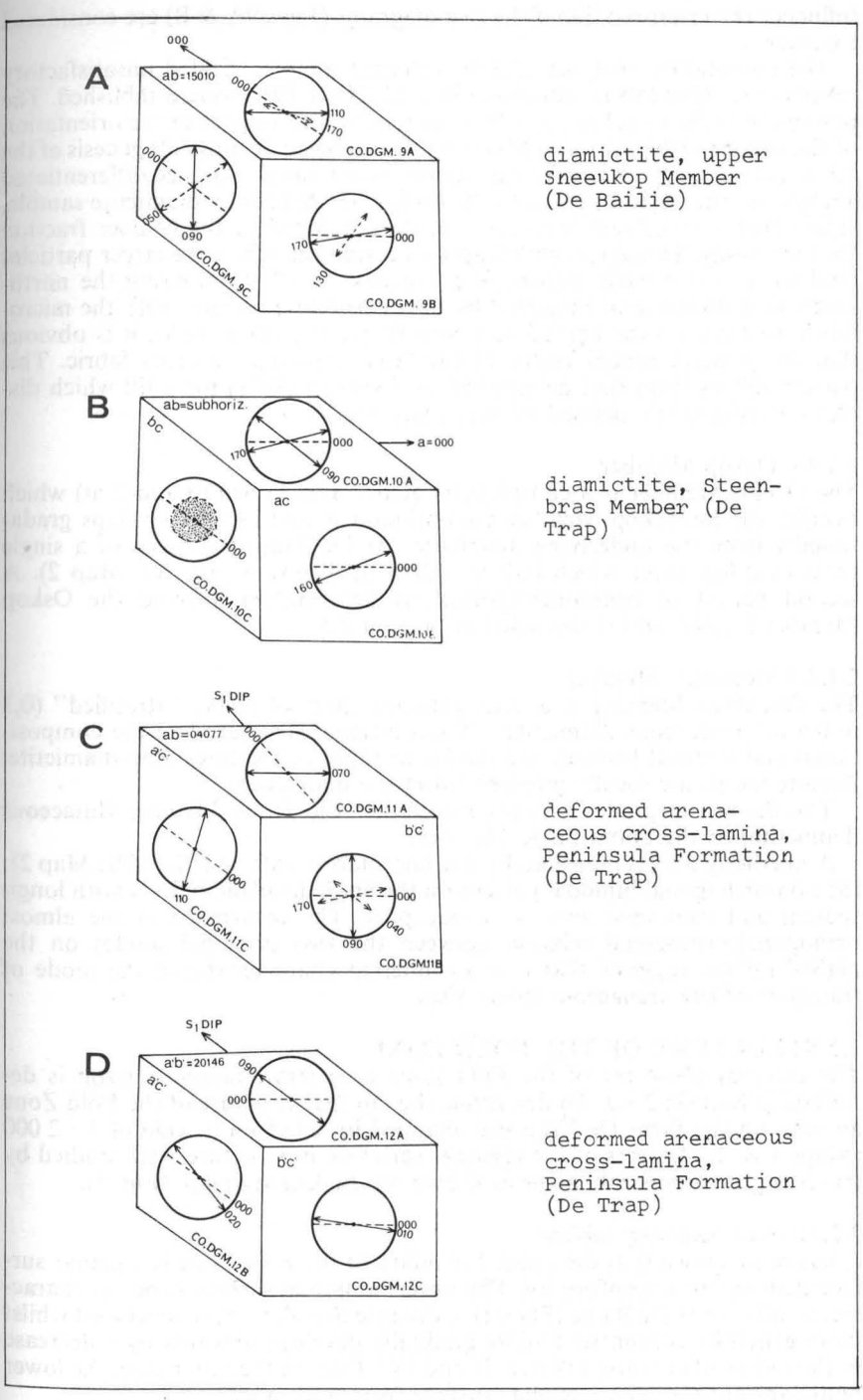

Fig. 10. Three-dimensional microfabric patterns as defined by the preferred orientation of quartz grain long axes. Sample localities 10A to 10D are shown on Map 2.

influence the interpretation if the two diagrams (Figs. 9A & B) are considered together.

The microfabric analyses of three oriented samples yielded unsatisfactory results as triclinic fabric patterns (Figs. 7C, 7D & 10A) were established. The possible introduction, here, of a 10° uncertainty with respect to the orientation of the surface of deposition, adds an extra variable to the possible genesis of the fabric pattern and renders further interpretation futile. The size differentiated analysis on the ab(Sed.)-plane (±10°) (Figs. 7D & 11) of a diamictite sample, shows that a significant transverse mode developed in the coarser fraction (≥ 1 mm) only. This agrees with fluid-flow conditions where the larger particles tend to be transversely transported (Rusnak, 1957). Comparing the north-south flow direction as indicated by the microfabric pattern, with the microfabric patterns on the ab(Sed.)-sections (Figs. 7C, 7D & 10A), it is obvious that the primary modal vector in each case represents a cross fabric. This pattern differs from that determined by Evenson (1971) for a fill which displays a cross fabric defined by secondary modes.

2.1.4.4 Oskop Member

The Oskop Member is a conspicuous quartz arenite bed (0,6 m-2 m) which overlies the Sneeukop Member discontinuously and locally develops gradationally from the underlying diamictite. At De Trap it consists of a single cross-stratified layer which indicates flow in direction 210° (cf. Map 2). A second period of penecontemporaneous deformation affected the Oskop Member locally, and is discussed in Section 2.3.

2.1.4.5 Steenbras Member

The Steenbras Member is a discontinuous sheet of feebly "stratified" (0,3 m-0,6 m) arenaceous diamictite without internal structure and the compositional and textural features are similar to those of the Sneeukop diamictite. Arenite lentils are locally interbedded in the diamictite.

The diamictite grades upward into either the Kobe Member (lutaceous diamictite) or the Soom Shale Member.

A northerly flow is indicated by one microfabric pattern (Fig. 10B; Map 2); the non-orthogonal bimodal pattern on the ab(Sed.)-plane reflects both longitudinal and transverse modes of transport. The recurrence of the almost orthogonal/orthogonal relation between the two principal modes on the ab(Sed.)-plane suggests that it is an inherent characteristic of the mode of transport of the arenaceous diamictites.

2.2 STRUCTURE OF THE FOLD ZONE

The external geometry of the Fold Zone as a stratigraphic horizon is described in Section 2.1.3. To determine the internal structure of the Fold Zone an area on the farm De Trap was mapped in detail on a scale of 1 : 2 000 (Maps 1 & 2). Aspects of the regional variation in structure were studied by traversing three separate areas as shown on the locality map. (Fig. 1).

2.2.1 *Lower bounding surface*

It has been shown that the upper boundary of the Fold Zone is a planar surface defining an unconformity. The lower bounding surface varies in character; locally, as at De Bailie (Plate I), a discrete décollement is developed whilst more generally concentric folding gradually develops upwards by a decrease in the radius of curvature (Plates II and IV). Even in the latter case, the lower boundary appears like a regular surface from a distance.

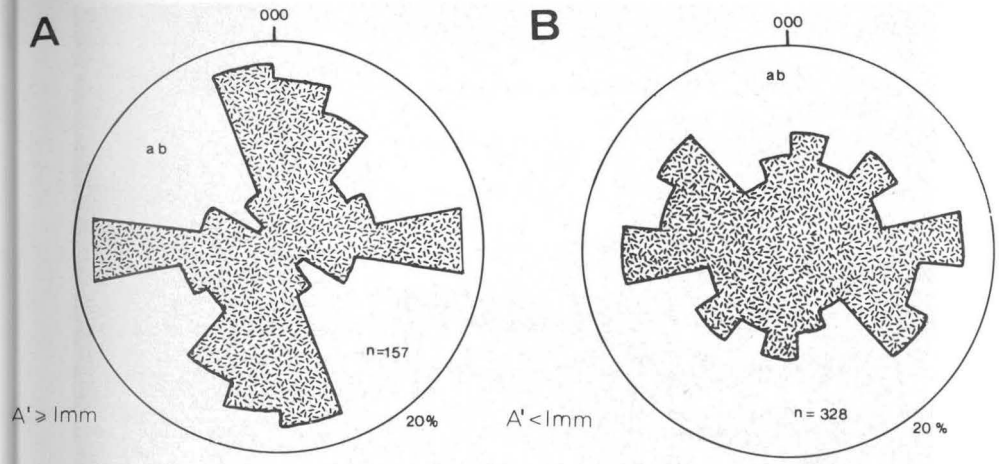

Fig. 11. A size differentiated analysis on the ab (Sed)-plane of a sample from the upper Sneeukop diamictite. The transport medium was such that a significant orthogonal bimodal pattern developed only in the coarser sand-sized fraction (cf. A and B). The three-dimensional pattern is shown in Fig. 7D.

2.2.2 *Prominent Fold Zone features*

A striking characteristic of the Fold Zone is the variation in character and thickness of the folded layers. In the bottom portion of the zone or where the interlimb angle is large, the typical cross-stratified layers of the Peninsula Sandstone are recognizable as such. Towards the top though, the buckled layers are commonly thinner and are internally 'laminated' parallel to the layering. It has been established (Section 2.2.4) that the change takes place due to rotation of the cross-laminae.

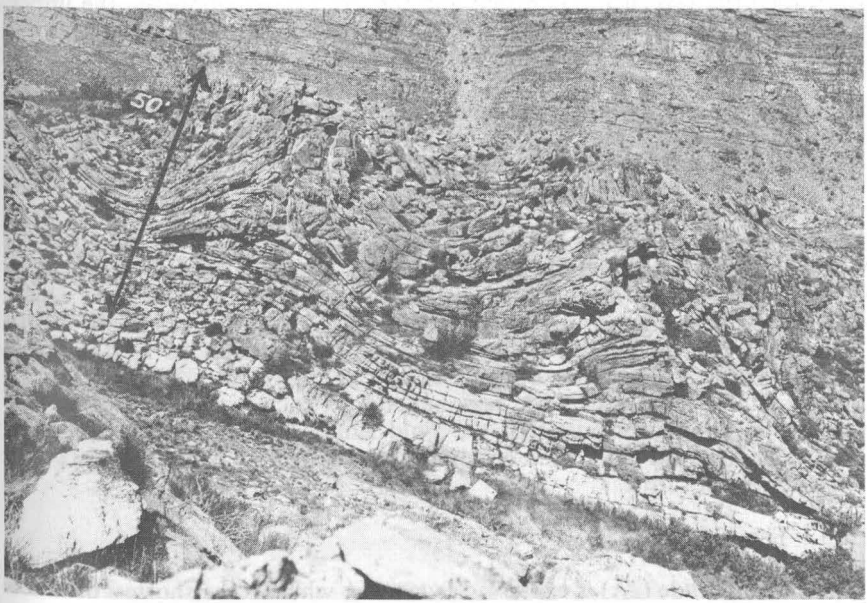

PLATE IV
Close-up view of the Fold Zone at De Bailie.

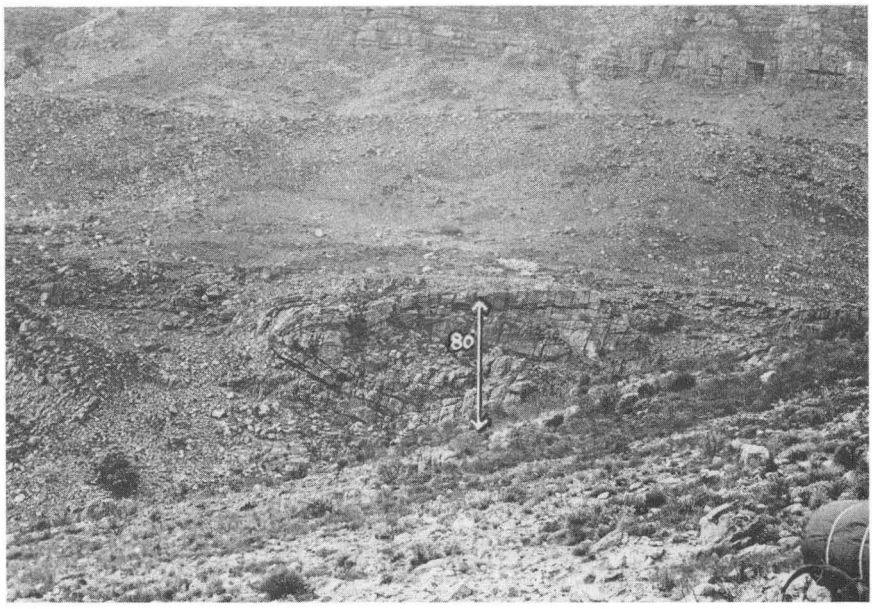

PLATE V
A recumbent fold at Patryskop; the upper limb forms the top of the Fold Zone.

Another notable feature observable in profile, is that both upright and overturned folds are developed (cf. Plates I, II, IV and V); all gradations from upright to isoclinal recumbent folds were observed. Where the folds are overturned the vergence is constant and the axial traces approach the upper boundary of the Fold Zone tangentially from an upright attitude along the bottom of the Fold Zone; the two general cases are illustrated in Fig. 12.

An aspect of style which was observed without exception is the narrow cuspate forms of anticlines and the broad rounded shapes of synclinal hinge zones (Plate II).

Canoe-shaped folds are prominently developed in some areas; elsewhere individual folds remain cylindrical for at least hundreds of metres along strike.

2.2.3 *Description of structures*

Maps 1 and 2 depict the Fold Zone as seen on an oblique erosional surface. Synclinal depressions are occupied by the lower Sneeukop diamictite which shows a sporadic outcrop pattern due to the non-cylindrical character of the folds. The relative stability of the fold axial trace directions in domain 2 (Map 2) contrasts with the obvious effects of interference folding seen in domains 3 and 4. Considered in regional context such a cross fold pattern is not a common characteristic of the Fold Zone. Domain 1 represents the lower portion of the Fold Zone where the intensity of deformation markedly decreases downwards.

2.2.3.1 The Folds

Fold dimensions

(i) The amplitude (2A) is expressed by a value which is the shortest distance between the enveloping surfaces of a folded surface. For the different folded surfaces, 2A varies from top to bottom in the Fold Zone and

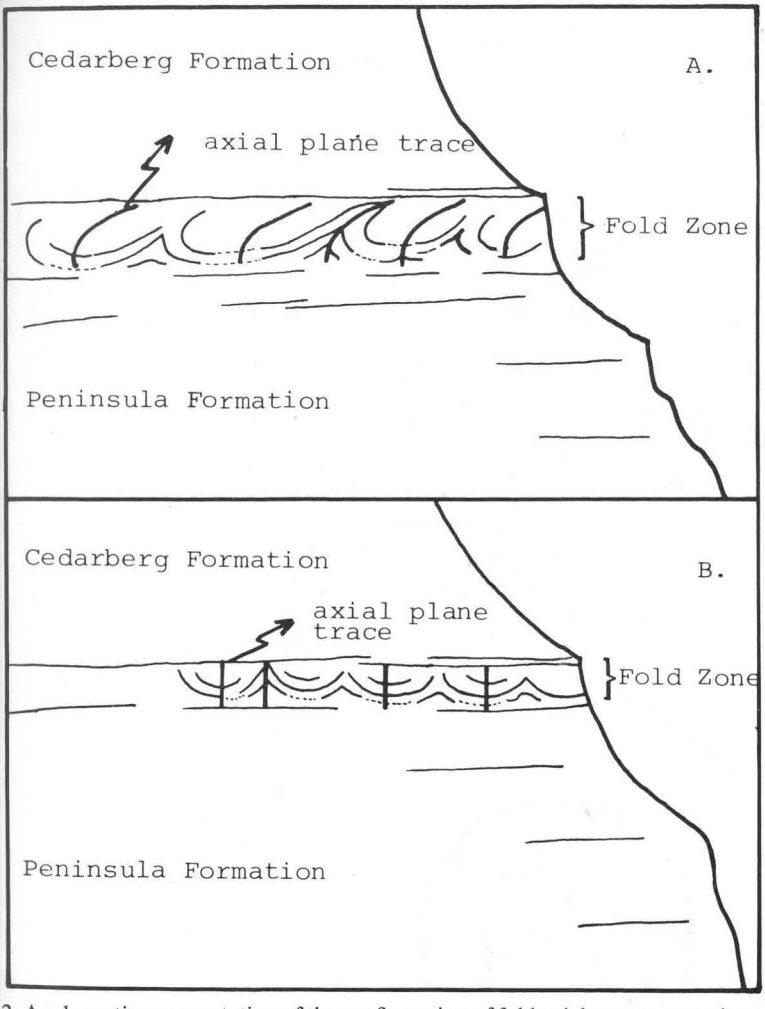

Fig. 12. A schematic representation of the configuration of fold axial traces as seen in profile. A. Axial traces become inclined towards the top of the Fold Zone. B. Towards the proximal margin of the Fold Zone axial traces remain subvertical from top to bottom.

commonly increases stratigraphically upwards (Plates II and IV). For synclines, especially in the intensely deformed areas, 2A approaches the Fold Zone thickness (Plate I); a maximum value for 2A thus inferred is 200 ft-250 ft (60 m-80 m). The areal variation of 2A will therefore also parallel the trend of the Fold Zone thickness (Figs. 13 and 14).

(ii) The wavelength (λ) is approximated by the crestal distance (λ') between adjoining anticlines (or synclines) parallel to the enveloping surface of the Fold Zone. Areally, λ' varies considerably, ranging from 35 ft to 350 ft (10 m-100 m). At De Trap (Map 2) λ' is fairly constant, generally varying from 30 m to 60 m (cf. Fig. 15). A scatter diagram (Fig. 20) shows no relation between Fold Zone depth and λ'.

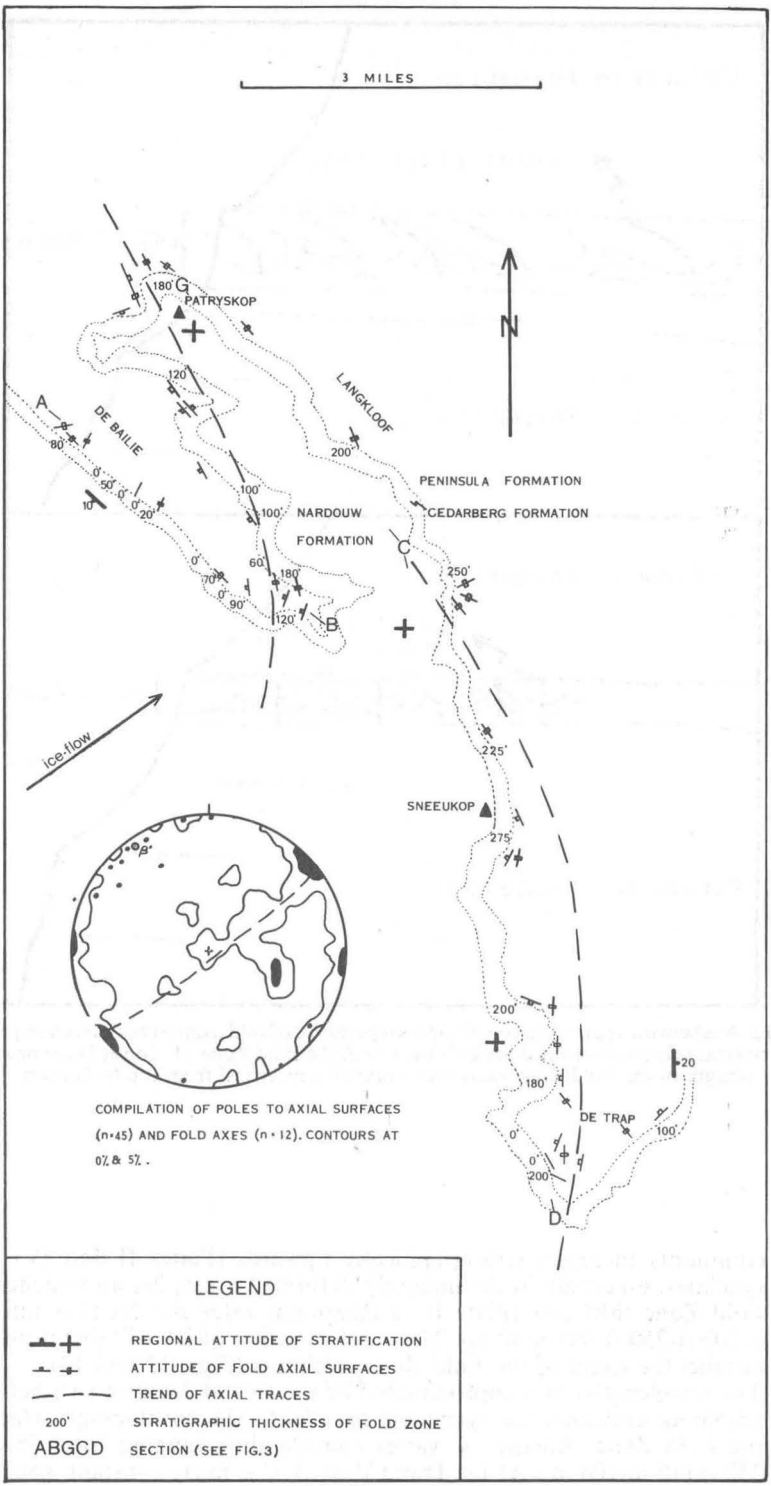

Fig. 13. Regional fold configuration and thickness of the Fold Zone in the De Trap/Patryskop area.

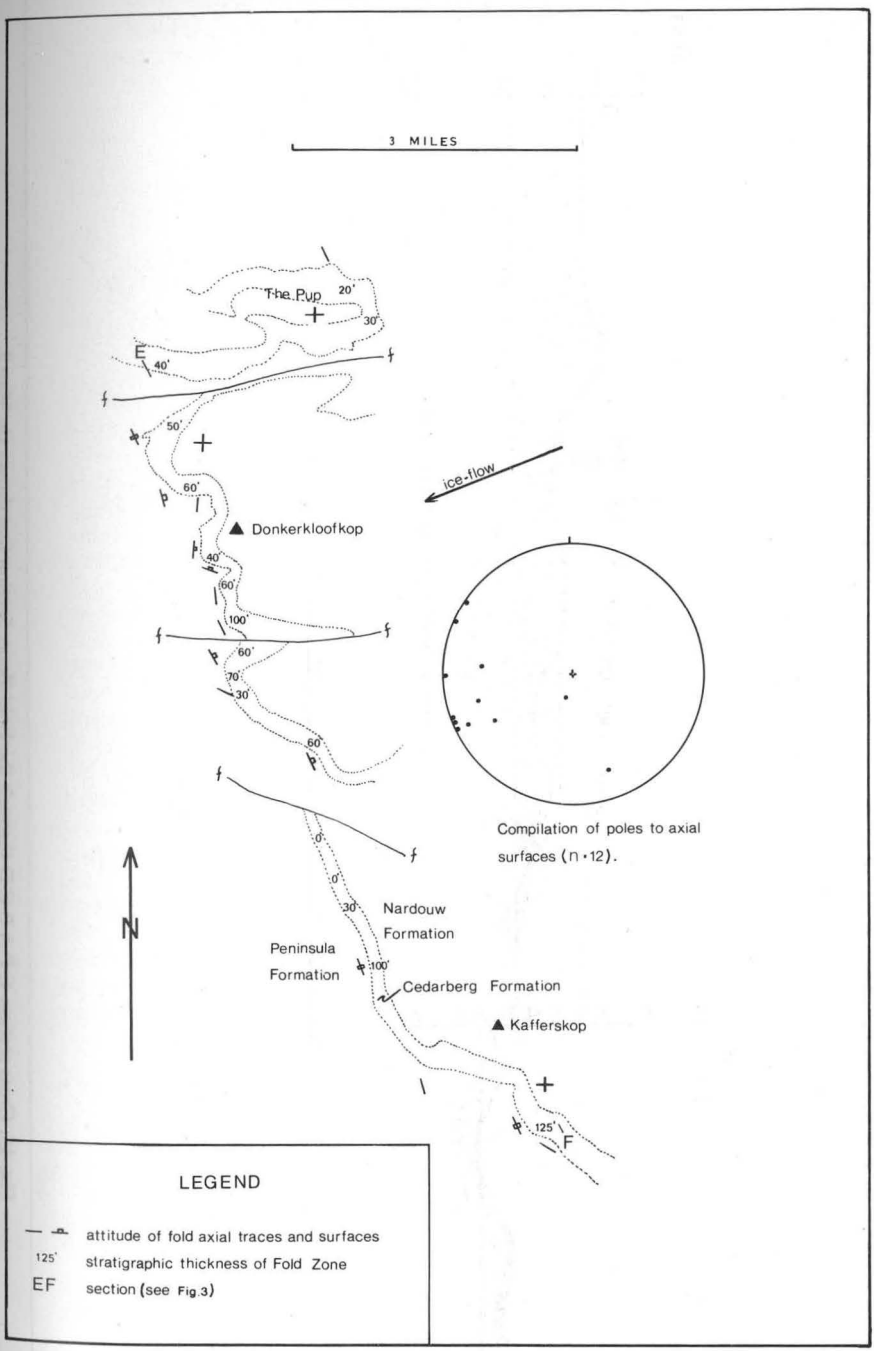

Fig. 14. Regional fold configuration and Fold Zone thickness south of The Pup.

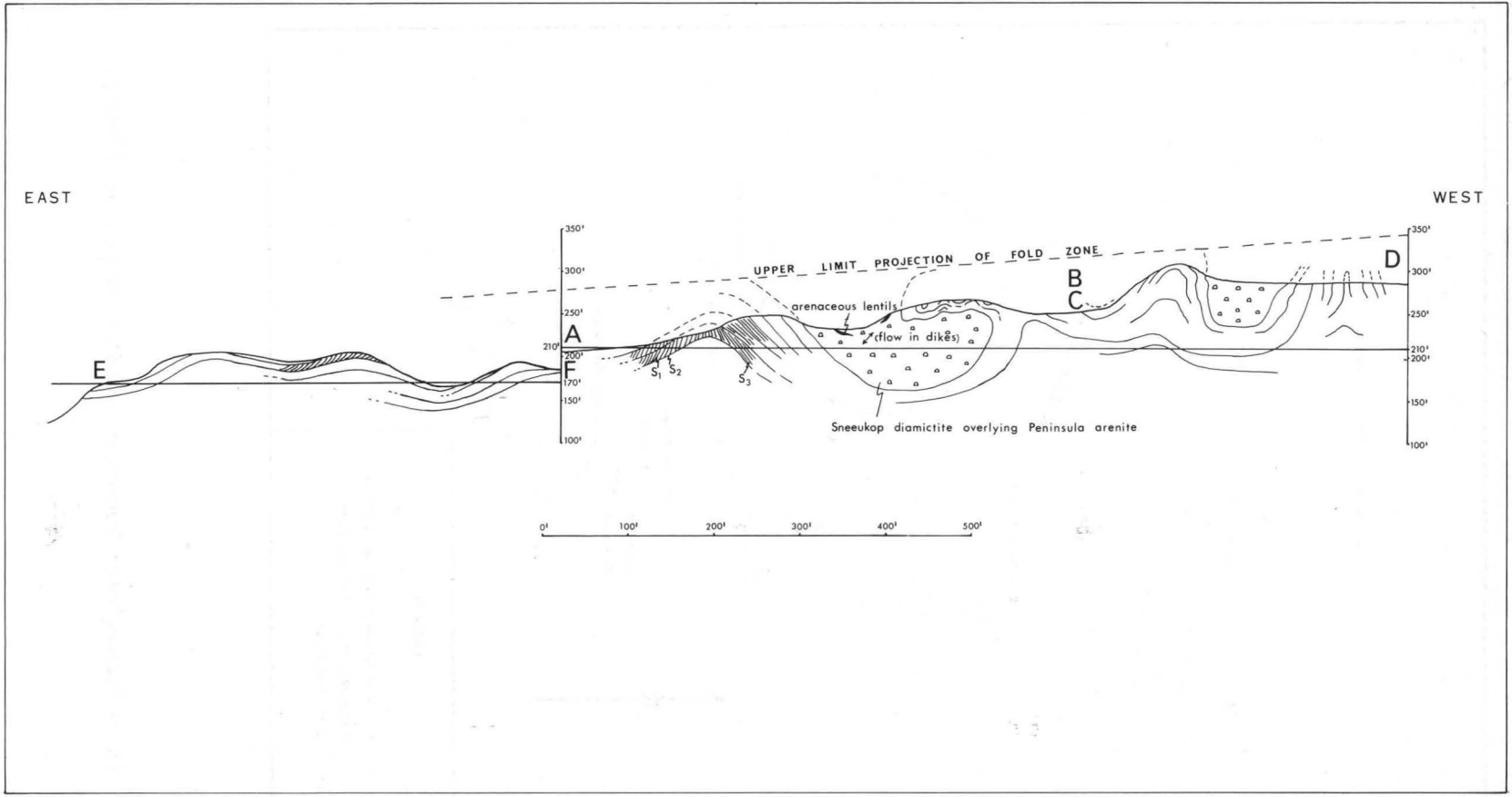

Fig. 15. Cross section E F A B C D through the Fold Zone. Section line shown on Map 2.

(iii) Continuation along fold axis. The detail map at De Trap discloses that some individual synclines or anticlines continue for at least 2 000 ft (600 m) along their axes. The pod or canoe-shaped folds which have definite closures normal to their axes, have the following long dimensions:
Karookop 60 m, 120 m, 180 m, 300 m.
Donkerkloof 60 m, 90 m.

In profile

The fold interlimb angles increase downwards for successively folded surfaces (Plate IV). Isoclinal folds, or even elasticas-like (interlimb angle $\theta < 0$) synclines, where developed, are situated in the upper portion of the Fold Zone.

The shape of folds in profile is illustrated by the cross-sections (Figs. 15-19) constructed from Maps 1 and 2. Compare also Plates I, II and IV. The characteristic features are listed below.

(i) The radius of curvature increases downwards to a horizon of no deformation, which may be a detachment zone.
(ii) Folded layers are markedly thickened in the cores of anticlines, but remain attenuated in the synclinal hinges.
(iii) Second or higher order folds on the limbs of major folds are scarce.
(iv) The contrasting profiles of anticlines and synclines is the most striking aspect of style; small tightly folded anticlines, commonly with angular hinge zones, are situated between considerably broader synclines which may bulge downwards where overfolded. The synclinal hinge zones are typically broad and rounded and contrast as such with the narrow cuspate anticlines.
(v) Judging from the shape of folded layers, subsimilar folds are developed in the upper portion of the Fold Zone whereas lower down the folds approach parallel-like shapes.

In three dimensions

Cross-folding features were observed at De Trap (Map 2, domains 3 and 4) only and are not thought to be commonly developed on a regional scale.

From Patryskop northwards, i.e. towards the Fold Zone margin, canoe-shaped folds or pod folds (Plate VI and Fig. 21) become common. Their length/breadth ratio, based on five measurements, is approximately 3,4; breadth being the distance between inflection points on adjacent limbs. The

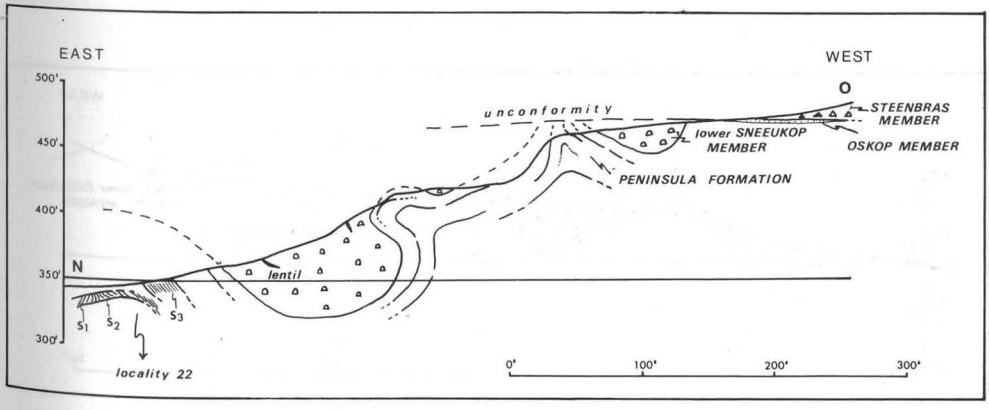

Fig. 16. Cross section N O through the Fold Zone.
Section line shown on Map 2.

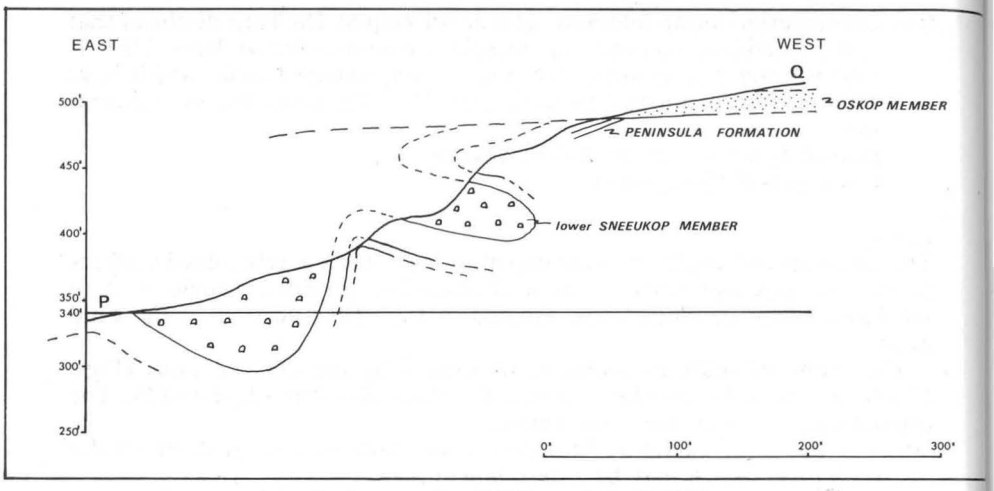

Fig. 17. Cross section P Q through the Fold Zone.
Section line shown on Map 2.

pod folds are generally upright, but were also observed to be overfolded; in some instances even the long end closures are slightly overfolded.

Elsewhere individual folds are thought to be cylindrical for at least hundreds of metres along strike, but remain non-cylindrical on a larger scale.

2.2.3.2 Small Structures

(i) *Minor folding* in the layering (S_4-bands) is rare and mostly congruous with respect to the first order folds. More common are congruous minor folds in S_3-bands within S_4-bands:

(*a*) Some are parasitic to folding in S_4-bands. (Plate VII A and B).

(*b*) Other geometrically incongruous minor folds probably formed during the transposition of the cross-laminae (Plate VIII).

(*c*) The asymmetry of the minor fold (Fig. 4G) positioned along the hinge zone of an anticline is inconsistent with minor fold development during buckling and was probably formed prior to the anticline by a component of simple shear across the S_4-band.

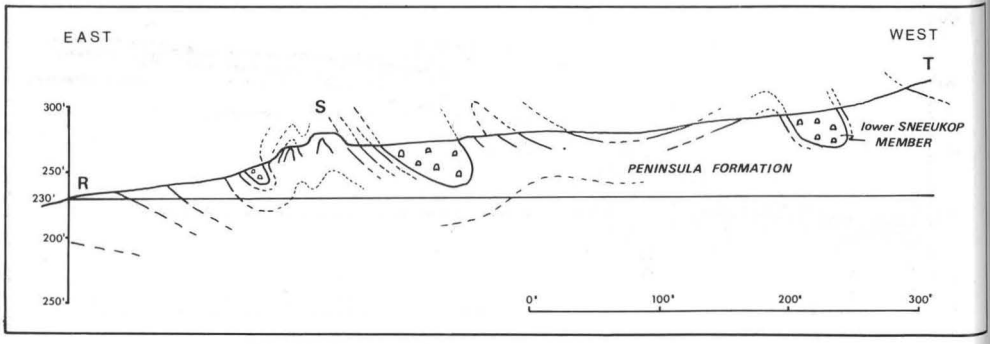

Fig. 18. Cross section R S T through the Fold Zone.
Section line shown on Map 2.

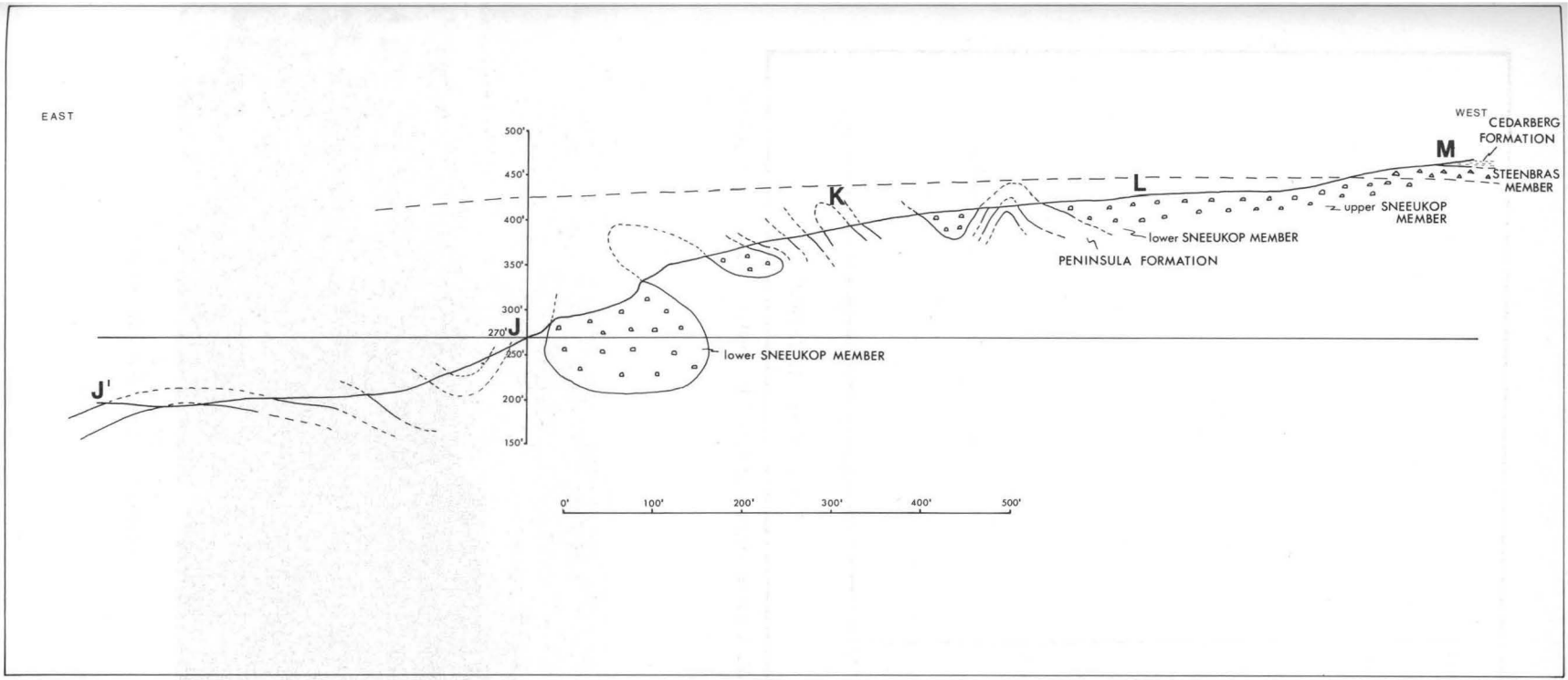

Fig. 19. Cross section J'J K L M through the Fold Zone. Section line shown on Map 2.

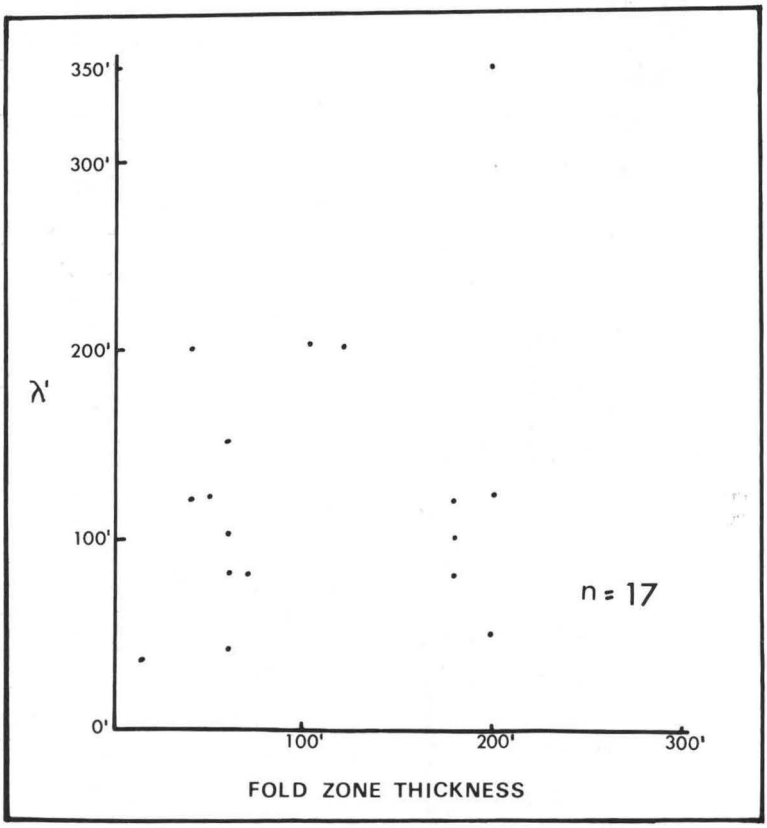

Fig. 20. A scatter diagram of Fold Zone thickness against fold width (λ′).

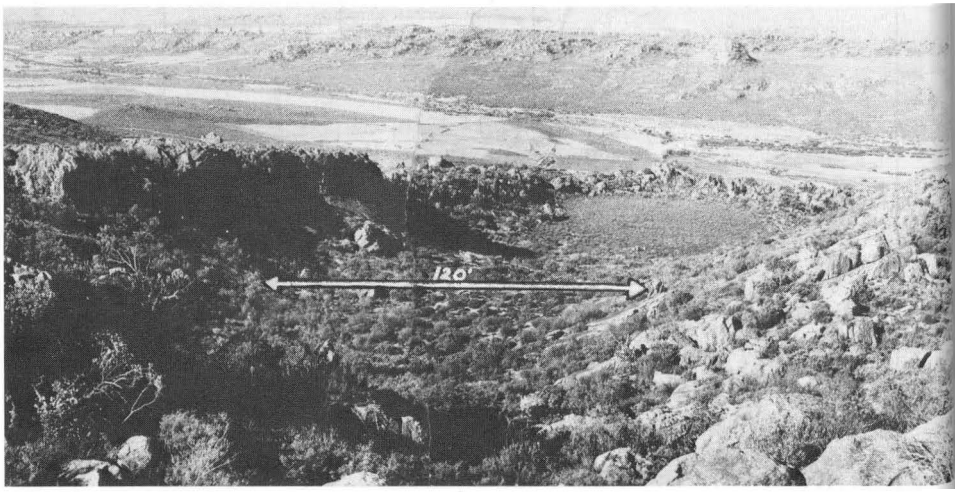

PLATE VI
An asymmetric pod fold (Karookop).

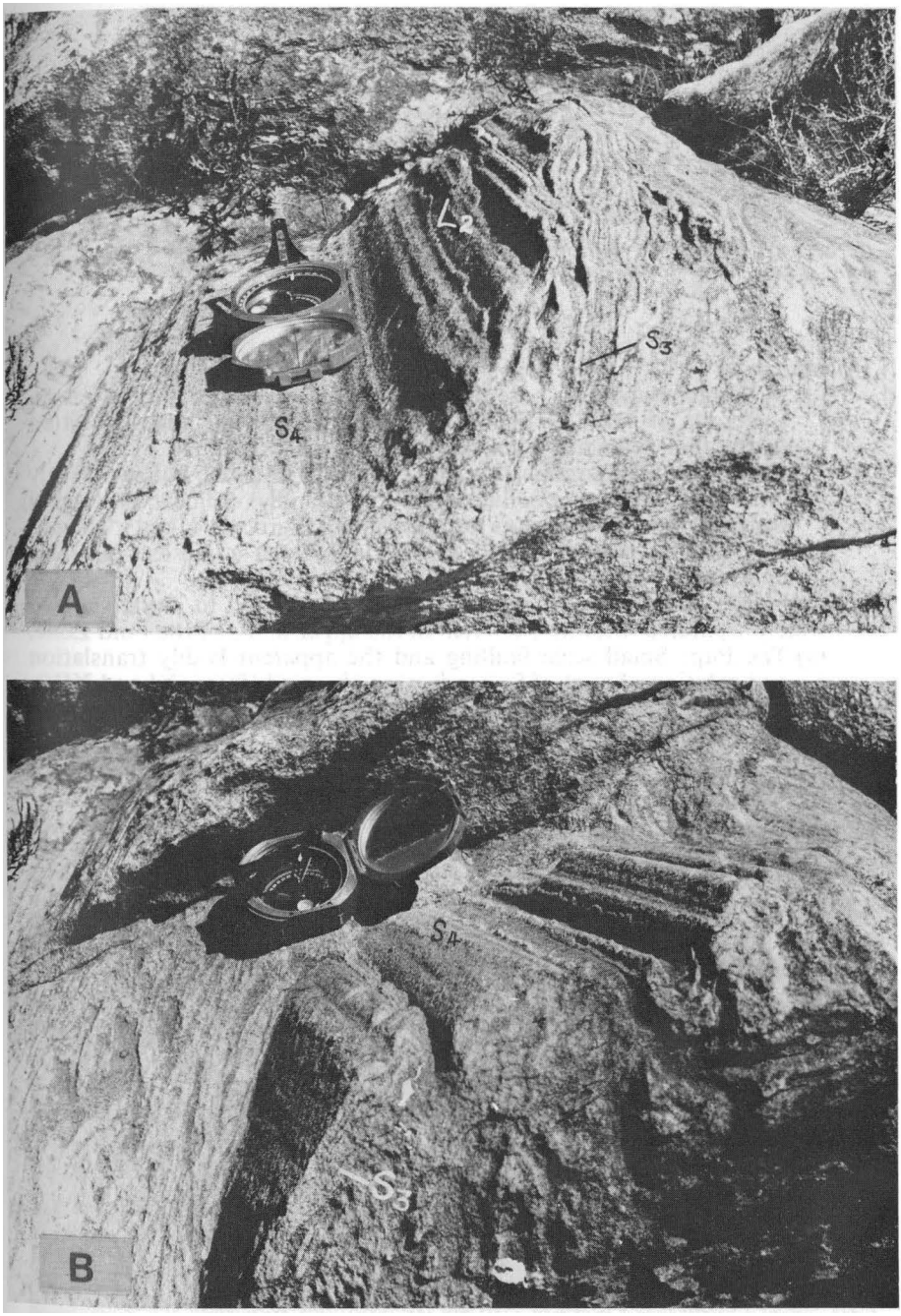

PLATE VII A AND B
Minor folding in rotated/transposed cross-laminae (De Trap).

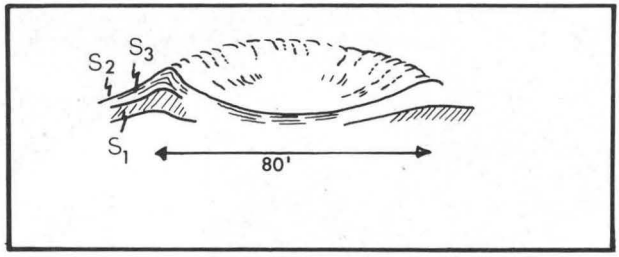

Fig. 21. The end-on closure of a pod fold.

(ii) *Lineations*

(*a*) S_1/S_2 intersections (L_1) are primary and yield b(Geom.)-lineations on the crests of box-like folds as well as lineations not directly related to the fold geometric axes (Plate IX; Fig. 22).

(*b*) The most abundant lineation, L_2, is difficult to define but apparently is an S_3/S_4 intersection. It commonly resembles a linear parting of S_3-bands and also occurs as alternating "grooves" and "ridges" (Plates XA and B). Rarely it is curvilinear on a mesoscopic scale and macroscopically defines B (Figs. 23 and 24).

(iii) *Structures due to rupture* are rare and were observed to cluster at two widely separated localities, situated in the upper limits of the Fold Zone.

(*a*) The Pup: Small scale faulting and the apparent bodily translation and rotation of a set of S_3-bands were observed (Plates XI and XIV)

(*b*) De Trap: Faulting is associated with plastic behaviour as shown by the sympathetic folding of S_3-bands (Fig. 4H).

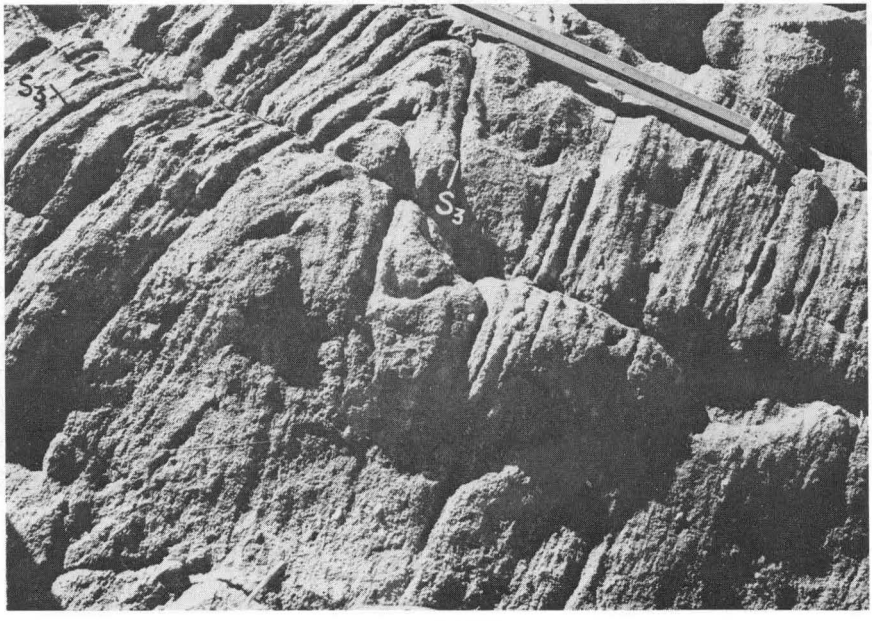

PLATE VIII

Subsimilar folds formed during the transposition of the cross-laminae; these folds are geometrically unrelated to the larger scale flexural-slip folds (De Trap).

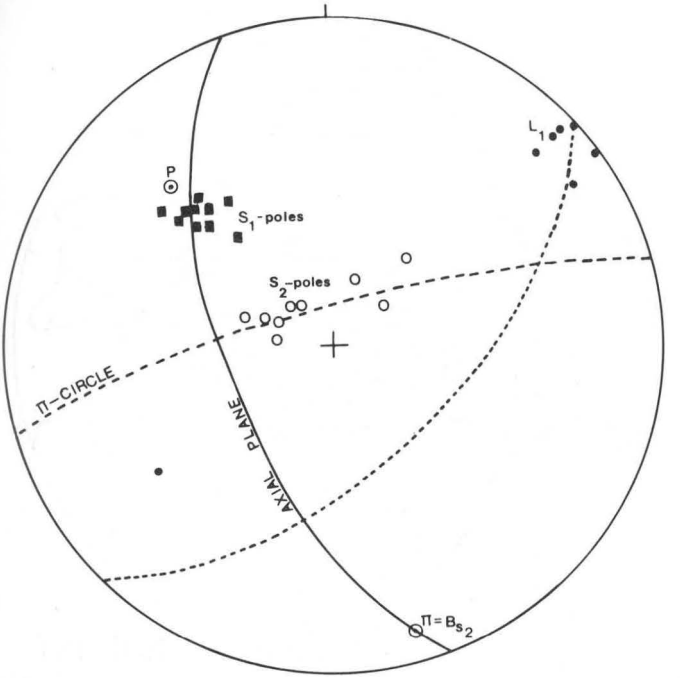

Fig. 22. The geometric relation between S_1, S_2 and L_1; data are from an anticline in the lower part of the Fold Zone (De Trap).

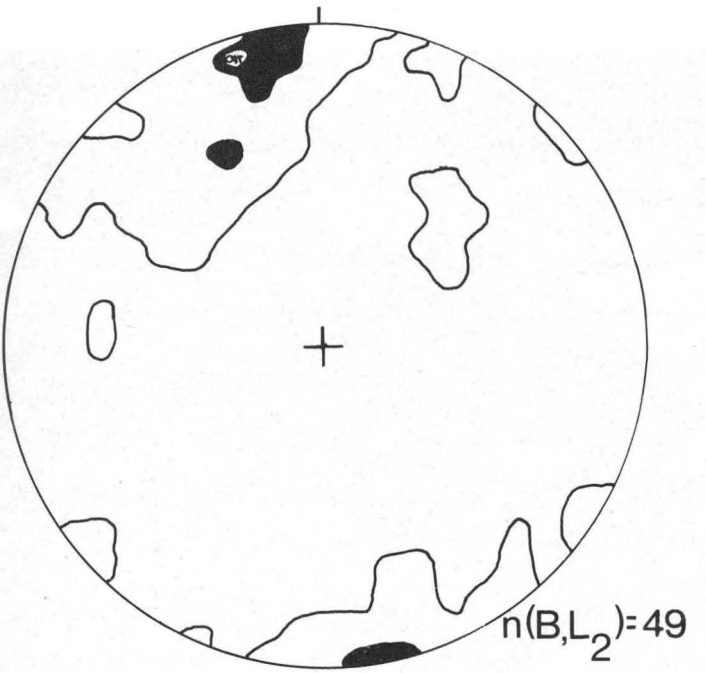

Fig. 23. A compilation of mesoscopic fold axes and L_2 in domain 3 (Map 2, De Trap); the π-pole is from Fig. 31. Contours at 0% and 10%.

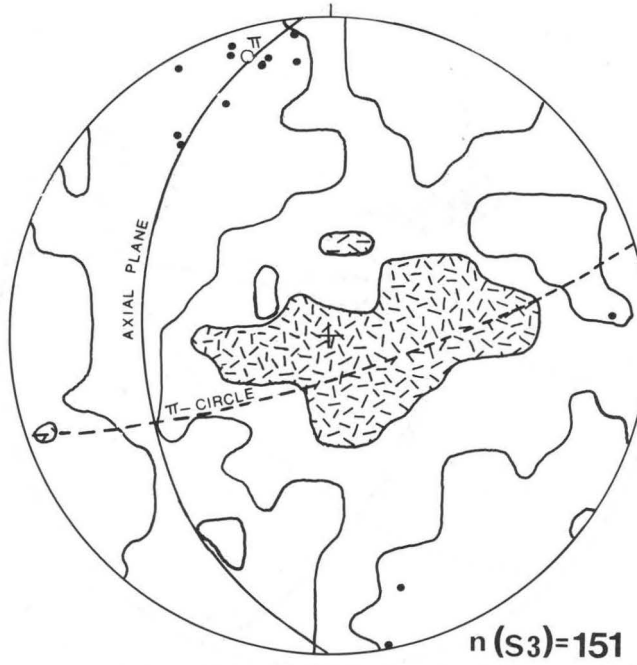

Fig. 24. The geometry of the Fold Zone subfabrics (S_3-poles, fold axes and L_2) in domain 2 (Map 2, De Trap). Contours at 0% and 3%.

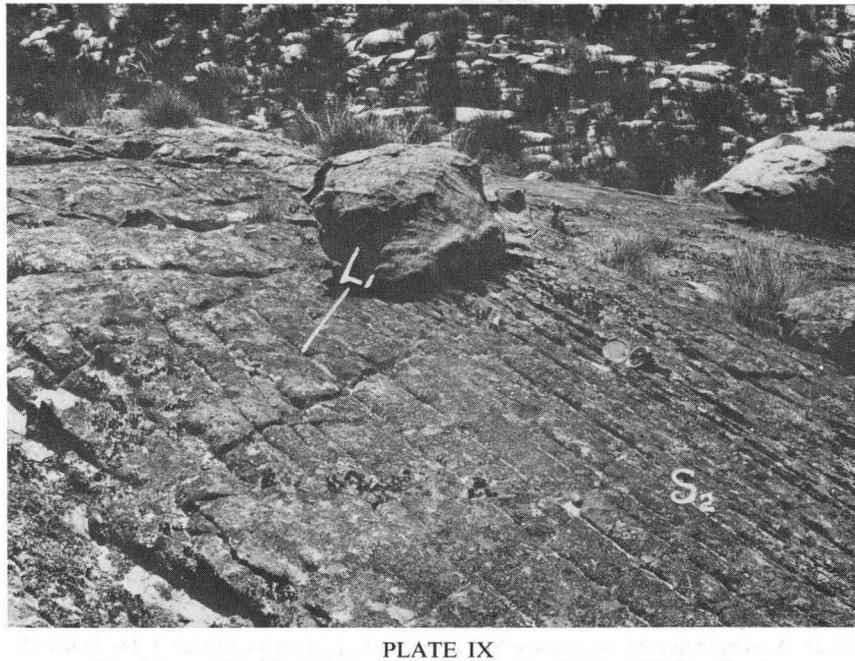

PLATE IX
The intersection of cross-laminae with the stratification (S_2) (De Trap).

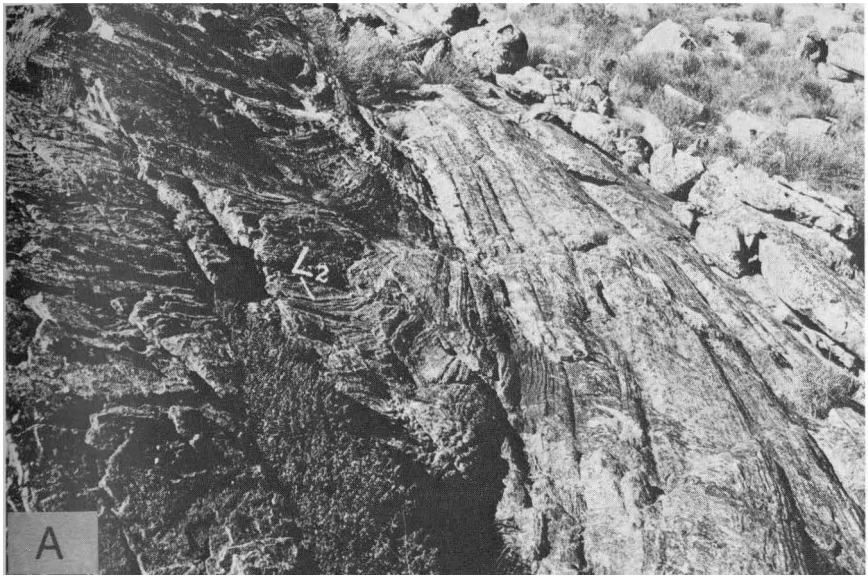

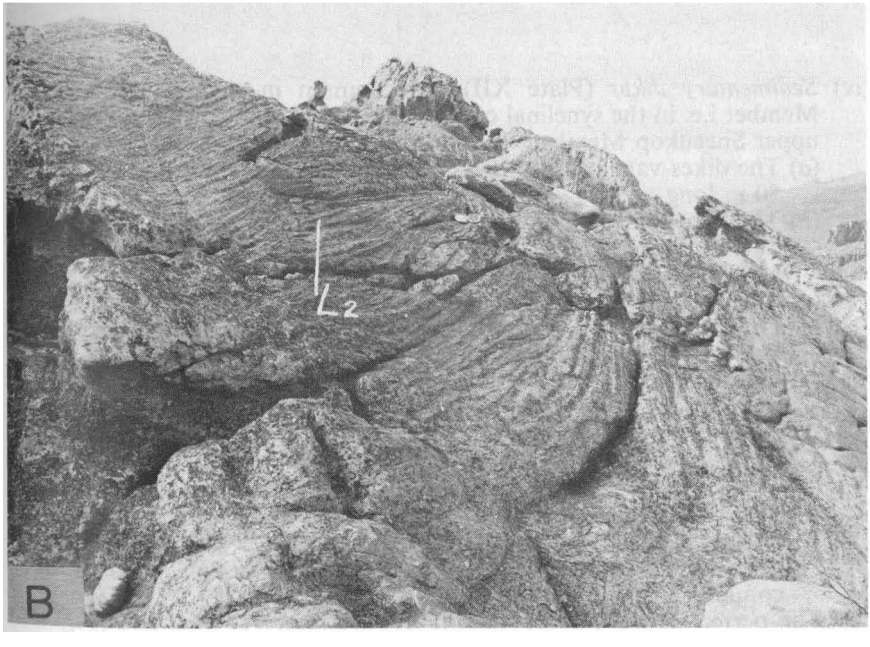

PLATE X A AND B

The lineation, L_2, is developed only where the cross-laminae are completely transposed (Langkloof and Sneeukop).

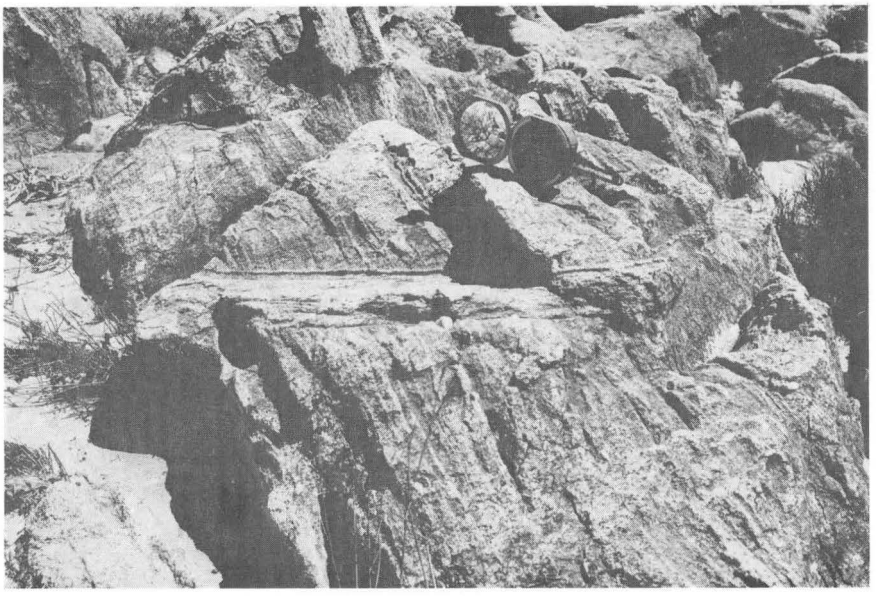

PLATE XI
An enigmatic structure (The Pup).

(iv) *Sedimentary dikes* (Plate XII) are common in the lower Sneeukop Member i.e. in the synclinal cores (Map 1) and were not observed in the upper Sneeukop Member. They have the following characteristics:

(*a*) The dikes vary in width from 2 cm to 35 cm and are from 1,5 m to 30 m long.

(*b*) They are slightly curvilinear, frequently bifurcate and usually taper out; a single example of abrupt termination against the Peninsula arenite was observed.

(*c*) The dikes are always orientated normal to the synclinal axis.

(*d*) Grading along strike was observed; the coarser part of the dike being away from the Peninsula arenite contact.

(*e*) Grading across strike is common and was also observed microscopically within the sand-sized fraction. The coarser material is concentrated in the middle portion of the dikes, and commonly contains odd pebbles and grit.

(*f*) The contact between a dike and the surrounding diamictite is sharp.

(*g*) The compositional and textural features of the dike material are similar to those of the diamictite of the lower Sneeukop Member described in Section 2.1.4.2; euhedral pyrite, though, is much more common in the dikes.

The perfect orthorhombic microfabric symmetry of one dike (Fig. 25) is thought to be characteristic for quasi-liquid flow (Elliot, 1965) parallel to the dike walls. Assuming (after Bhattacharyya, 1966) parallel arrangement of linear grains with flow, a(Kin.) is defined as shown on Figs. 25 and 15 and Map 2.

A second dike yielded a triclinic fabric pattern (Fig. 26) which is probably due to flow, obliquely aligned with respect to the dike walls. Net flow, parallel to the dike walls, was apparently horizontal. Such flow can be ascribed to variance in the viscosity of the flow medium or to obstacles.

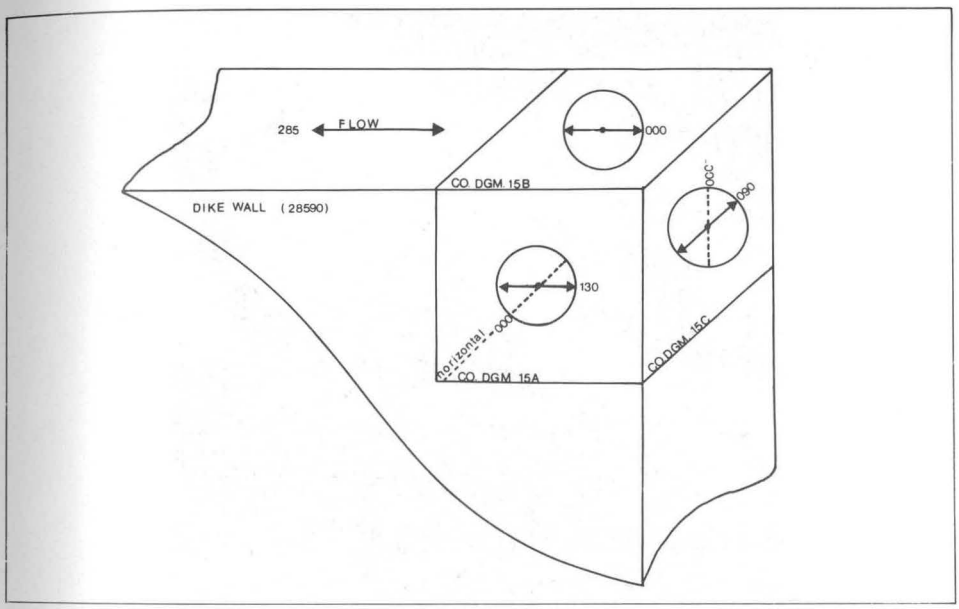

Fig. 25. The three-dimensional microfabric pattern defined by the preferred orientation of quartz grain long axes in a sedimentary dike from the lower Sneeukop Member, De Trap Locality 25 shown on Map 2.

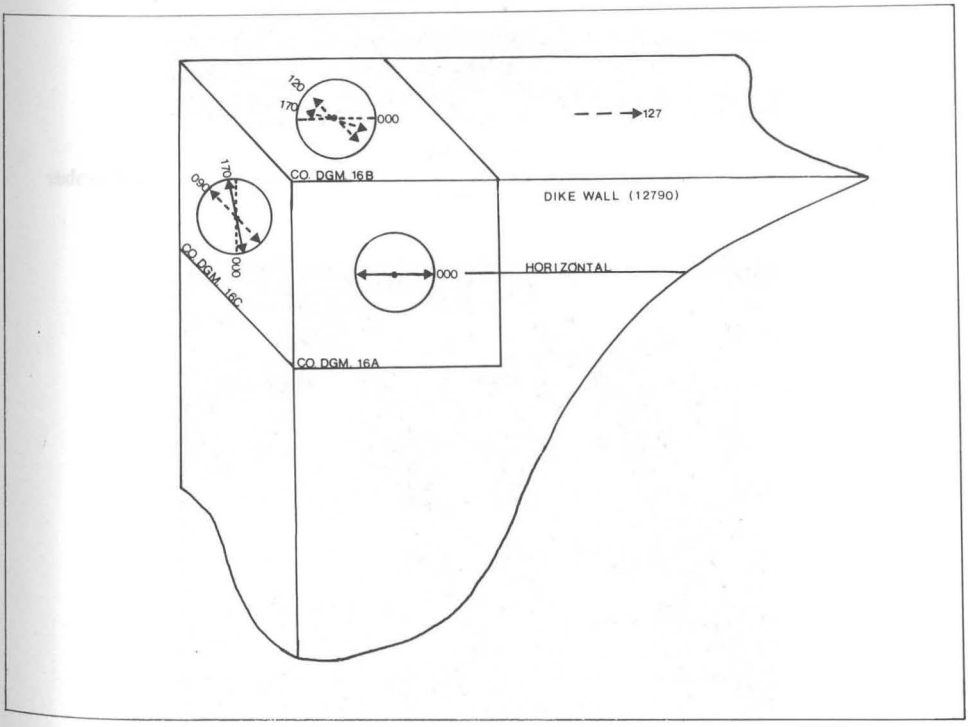

Fig. 26. The three-dimensional microfabric pattern defined by the preferred orientation of quartz grain long axes in a sedimentary dike from the lower Sneeukop Member, De Trap. Locality 26 shown on Map 2.

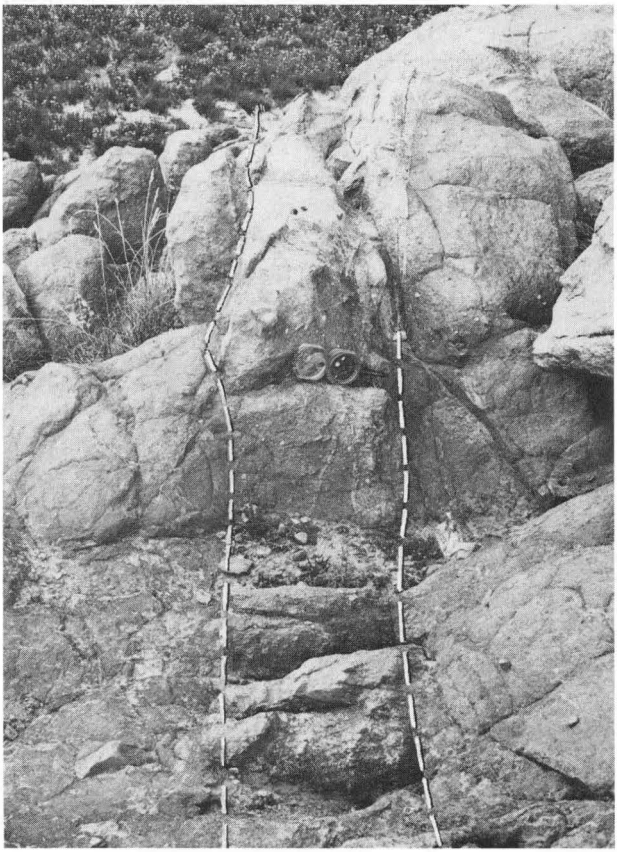

PLATE XII
A sedimentary dike, oriented normal to the fold axis, in the lower Sneeukop Member (De Trap).

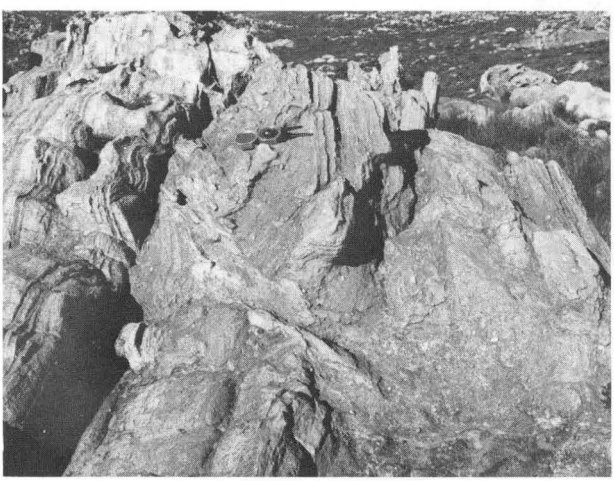

PLATE XIII
Detached bands of deformed Peninsula arenite within the lower Sneeukop Member (De Trap).

(v) *Detached and semi-detached bands* of Peninsula arenite are commonly situated in the lower Sneeukop diamictites at or near the contact. The arenite bands are easily recognized as of Peninsula origin by their transposition features. The bands range in length from 0,3 m to 12 m and are generally only 15 cm thick (exceptionally 1 m). Where abundant, the contact is rendered irregular by the mixing of the two rock components (Plate XIII). Map 1 shows that the bands are concentrated on the western contacts and culminations of the diamictite-containing synclines; the bands are generally aligned parallel to or tangential to the structural trend. Folding and buckling of detached arenite bands were observed. The detachment is thought to take place by splaying and by parting along S_3-surfaces of the Peninsula arenite.

2.2.4 *Rotation and transposition of cross-laminae*

During folding S_1 (cross-laminae) was rotated to varying degrees, the final arrangement being a function of the original orientation with respect to the fold geometry, the fold mechanism and the finite strain. In a rare box-like fold, S_1 tends to be parallel to the layering, S_2, on the limbs while it is perpendicular to the folded surface in the hinge zone (Fig. 4C). In another fold (Fig. 4D) S_1 maintains a large angle in relation to S_2 throughout the hinge zone.

A well exposed hinge zone at De Trap (Fig. 4E) allowed a detailed orientation study of S_1, S_2 and L_1. With respect to the fold elements, the sampled area constitutes a homogeneous domain. All possible attitudes of S_1, S_2 and L_1 were measured, and compiled on a Schmidt net (Fig. 22). The following features are evident:

(*a*) The orientation of S_1 remains virtually unchanged throughout the fold.

(*b*) L_1 is contained within a planar surface which approximately coincides with the average S_1 orientation. The varying attitude of L_1 within the surface is therefore only due to the folded nature of S_2.

(*c*) The S_1-pole point maximum lies within the axial surface of the anticline at an angle of 50° from the fold axis.

More observational data are needed to explain why, if not fortuitous, the cross-laminae are not folded, but planar normal to the axial surface.

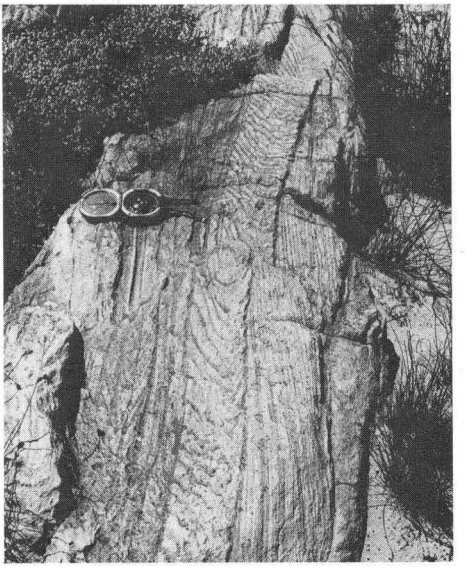

PLATE XIV

Penecontemporaneous faulting in the upper horizons of the Fold Zone (The Pup).

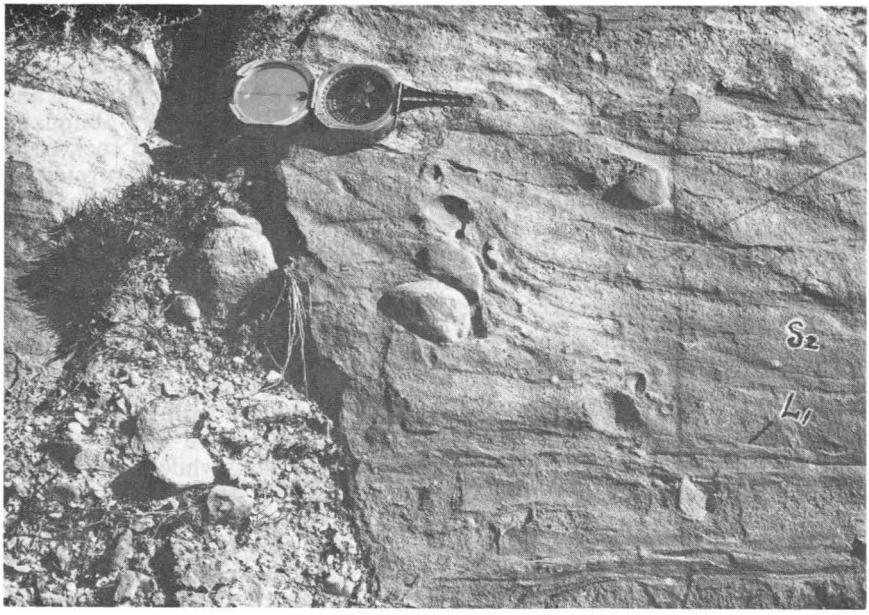

PLATE XV
Rotational drag on the stratification surface (facing reader) associated with the rotation/transposition process of the cross-bedding (De Trap).

The rotational features described above are typical of the lower portion of the Fold Zone. Towards the top of the Fold Zone cross-laminae are rotated to an attitude parallel to the folded layers, S_4, which contain sets of S_3-bands i.e. the transposed S_1. The S_4-bands probably represent the original stratification surfaces. Increased bulk strain towards the top of the Fold Zone would explain the generally thinner S_3-bands (0,1 cm-3 cm) in comparison with the thickness (1 cm-7 cm) of the cross-laminae towards the bottom of the Fold Zone. Some minor folds with geometries inconsistent with respect to the first order folds, are considered to have developed during the transposition process (cf. Fig. 4G and Plates VIII and XIV). The rotation process of S_1 was accompanied by rotation-drag of S_1 on S_2 as shown by the deformation of S_1 around obstructing pebbles situated in S_2 (Plate XV).

A single outcrop at De Trap (locality 27 on Map 2 and Fig. 16) displays the transposition process i.e. the rotation of the cross-stratification parallel to stratification (Plate XVI). Progressive stages in the rotation can be followed over 60 m within a bedding unit from left to right (Plate XVI and Fig. 4F) or from stage 1 through 2 to 3 where the transposition is complete. The cross-laminae are rotated through the vertical before they are flattened in the stratification surface with S_1 showing some thickening and folding as would be expected where S_1 is disposed subperpendicularly to S_2. The rotation of S_1 is not always through the vertical. In this particular example though, a significant component of simple shear acting along S_2 (Fig. 4F) is invoked to explain the rotation through the vertical.

The position of this rotation/transposition with respect to the first order folds, is shown in Fig. 16 (locality 27). Stages 1 and 2 are situated in the hinge zone of an anticline in the lower part of the Fold Zone, whereas stage 3 is situated more towards the limb of the adjacent syncline. The geometry of

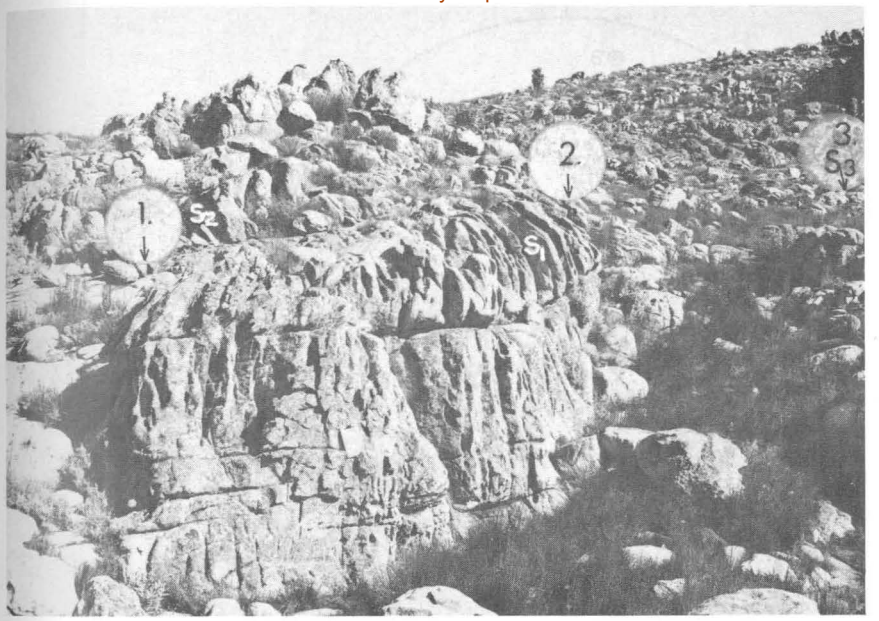

PLATE XVI

The different stages in the development of the rotation/transposition process; the final transposed stage, where the cross-laminae are parallel to stratification, has been attained between localities 2 and 3 (De Trap).

the rotation with respect to the fold axis is illustrated on Fig. 27. There is a 50° angle between the fold axis and axis of rotation, or a 40° angular distance between the plane containing the layer boundary shear directions and the fold axis. The sense of simple shear necessary to effect the rotation (Figs. 4F and 27) is consistent with the sense of layer boundary slip predicted by Ramsay (1967, p 392) for flexural-slip folding (cf. Fig. 16). The 40° angle between the layer boundary slip direction and the fold axis, means that the principal axes of bulk strain and the sand layers prior to folding were obliquely inclined with respect to each other (Ramsay 1967, p 396).

A microfabric investigation was conducted in order to learn more about the rheology of the sand at the time of deformation. For comparative purposes samples were taken at the outcrop discussed above, representing S_1 at different stages of transposition. The sample locations are shown on Plate XVI as 1, 2 and 3; the numbers also denote the transposition stages.

The *first stage* is represented by an S_1-layer in an early state of deformation before rotation through the vertical. The three-dimensional microfabric pattern as defined by quartz grain long axes, is depicted in Fig. 10C. The modal vector on a′b′(Sed.) is not symmetrically related to the dip direction (an indication of primary flow for undeformed cross-bedding) but tends to be transversely orientated. The large "imbrication" angle on a′c′(Sed.) suggests post-depositional deformation. Both the modal vectors on a′c′(Sed.) and b′c′(Sed.) are subperpendicular to the depositional interface. The low variance modes (refer to compass diagrams 11A and 11C in Blignault, 1970) indicate an imposed constraint on the rearrangement of grains.

The *second stage* is represented by an inverted S_1-layer after its rotation through the vertical. The three-dimensional fabric pattern (Fig. 10D) differs significantly from that of the first stage: (i) The modal vector on a′b′(Sed.)

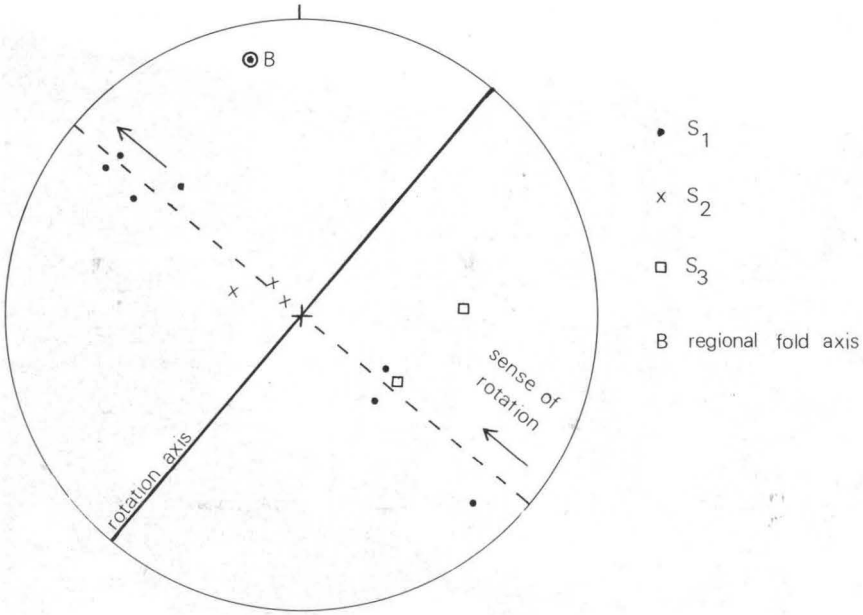

Fig. 27. The geometry of the rotation/transposition of S_1 towards S_2. The axis of rotation makes an angle of 50° with the synclinal fold axis.

parallels the dip direction or slip direction between S_1-layers (Fig. 27). (ii) The modal vector on a'c'(Sed.) now makes a small (20°) angle with the S_1-surface. (iii) A lower modal spread on all three planes of maximum fabric contrast is evident by comparing the relevant compass diagrams (Blignault, 1970) with those of the first stage.

The *final transposed stage three* is represented by an orientated sample taken from an S_3-band 60 cm from the arenite/diamictite contact and does not necessarily represent the same cross-stratified layer referred to above. The three-dimensional fabric pattern has essentially an orthorhombic symmetry (Fig. 28): (i) The modal vector on the S_3-surface makes a 10° angle with the dip direction i.e. it is subparallel. (ii) The modal vector on a'c'(Sed.) is parallel to S_3. (iii) The modal spread on the S_3-surface is significantly larger than those of stages 1 and 2.

By comparing the microfabric pattern of the three stages, the following is apparent: (i) The preferred orientation of quartz grain long axes within S_1/S_3 rotates mechanically from a transverse to a subparallel attitude with respect to the shear direction on S_1/S_3 (from Fig. 27 it is evident that the slip or shear direction between S_1 or S_3-bands is contained in the plane normal to the axis of rotation). (ii) The quartz grain long axes on cross-sections (with respect to S_1 and S_3 surfaces) become preferentially subparallel to S_1 and S_3 during progressive transposition; this is so because at stages 2 and 3, S_1 and S_3 are rotated into the elongation sector of the strain ellipse (Fig. 29).

It is concluded that layer boundary slip during flexural-slip folding and concomitant flow within layers (S_1 and S_3) caused mechanical rotation of quartz grains resulting in a new imposed quartz grain long axis subfabric. The low variance modal vectors describing the imposed subfabrics relate to a large shear strain.

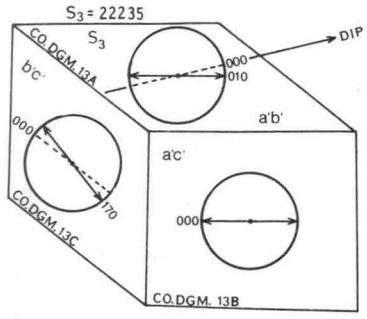

S3-band, Peninsula Formation (De Trap)

Fig. 28. The three-dimensional microfabric pattern (defined by the preferred orientation of quartz grain long axes) of a transposed cross-lamina (De Trap). Locality 28 shown on Map 2.

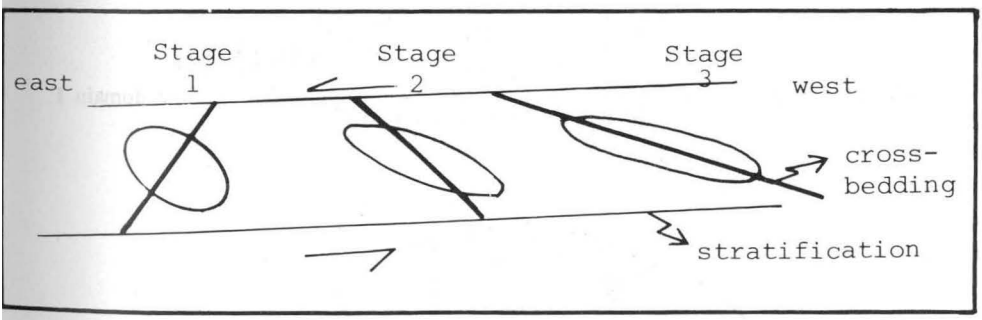

Fig. 29. A schematic illustration showing the relative change in orientation of the principal axes of the strain ellipse with respect to the changing attitude of the cross-bedding (cf. Fig. 4F). The progressive increase in the finite strain from stage 1 to stage 3 due to differential layer boundary slip during buckling, explains the different microfabric patterns developed at the three stages.

2.2.5 *Fold geometry at De Trap*

The configuration of fold elements in a portion of the Fold Zone at De Trap is presented on Map 2. The area is divided into four domains of least heterogeneity.

Domain 1 represents the lower portion of the Fold Zone and is the most homogeneous of the four; the S_2-pole girdle (Fig. 30) is ill-defined and indicates low-dipping fold limbs. The subhorizontally plunging mesoscopic fold axes are scattered about π. The S_2-pole girdle maximum and π define the preferred upright orientation of the axial surfaces.

Domain 2 is typical of an overfolded upper part of the Fold Zone. The distribution of S_3-poles has a large spread (Fig. 24); π forms the locus of the linear element distribution, and statistically L_2 is orientated parallel to the mesoscopic fold axes. Considered in conjunction with the cross sections (Figs. 16 and 17) the position of the maximum within the girdle indicates overfolding; the great circle through the minimum and π dips 40° west and

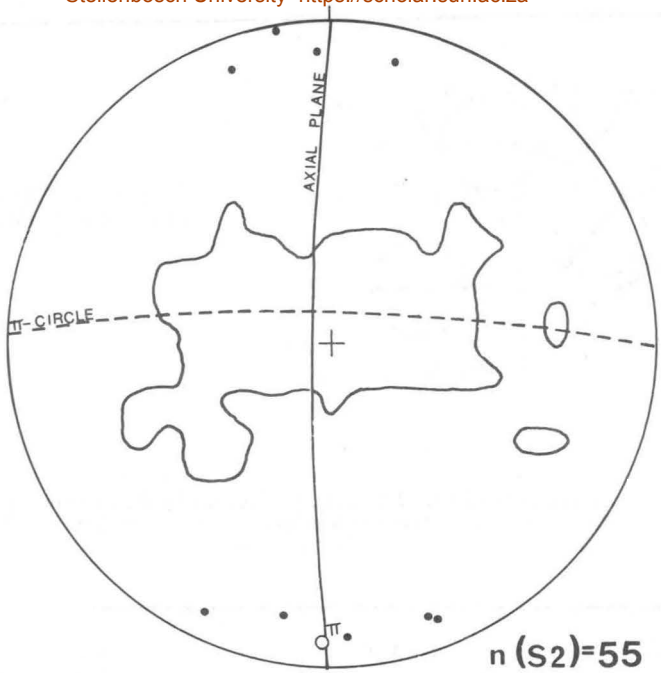

Fig. 30. Compilation of subfabrics (S_2-poles and mesoscopic fold axes) from domain 1 (Map 2, De Trap). Contour at 0%.

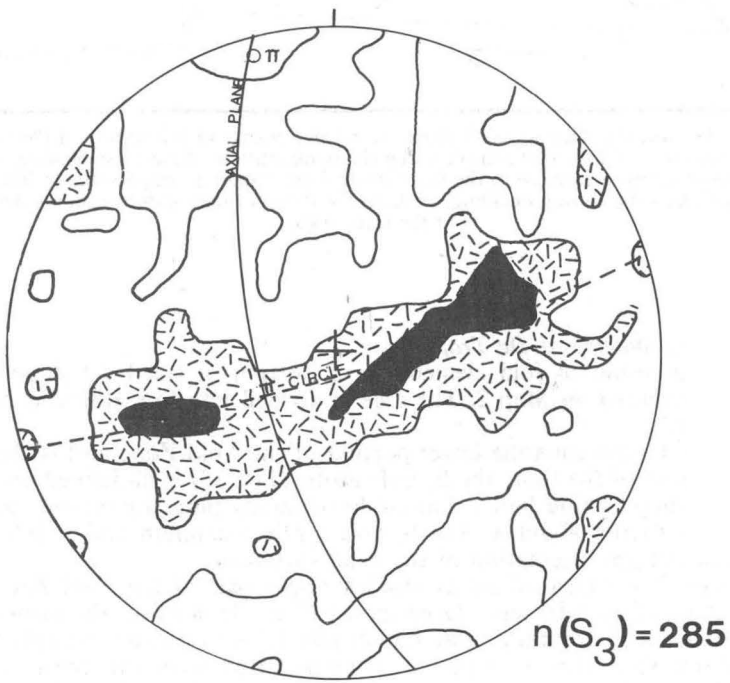

Fig. 31. Stereographic compilation of S_3-poles, domain 3 (Map 2, De Trap). Contours at 0%, 2% and 4%.

defines the preferred orientation of axial surfaces in domain 2. The axial trace thus inferred corresponds with the trend on the map.

Domain 3 comprises an area of more complex folding in the upper part of the Fold Zone. The stereographic compilation of S_3-poles (Fig. 31) shows a low direction stability. The π-circle is the best fit locus to the S_3-pole girdle. π, the preferred orientation of B, coincides with the locus of the linear elements (Fig. 23). Overfolding is less dominant and the axial surfaces preferentially dip 70° west.

Domains 3 and 4 together constitute an area characterized by a cross-fold pattern.

In summary, upright folds in the bottom portion gives way to overfolding with an eastern vergence in the upper part of the Fold Zone where linear elements preferentially plunge 5-10° in the direction 343°.

2.2.6 *Regional fold geometry*

From Patryskop and Langkloof northwards i.e. towards the margin of the Fold Zone canoe-shaped folds become common and the attitude of folds in the upper part of the Fold Zone is more generally upright than overfolded. At The Pup (towards the margin) pod folds approach near circular outcrop patterns and occur together with upright open folds. In the transitional area between overfolded and upright folds, it was observed that tight overfolding develops abruptly amongst adjacent upright folds; at one locality an upright fold was observed to develop into an overfolded isocline along the axial trace.

The regional traces of fold axes and axial surfaces are shown on maps (Figs. 13, 14 and 32) whilst the inferred regional pattern is shown on Fig. 1. The following characteristics are noted:

(i) From the stereographic compilation of fold elements from the De Trap/Patryskop area (Fig. 13) it is seen, firstly, that the axial surfaces, where close to the vertical, have varying dip directions but where inclined, they are preferentially orientated. Considered together, the poles are arranged around a zone axis β' which coincides with the locus of the fold axes; these linear elements plunge preferentially 5° in a direction 321° and the axial surfaces dip preferentially towards the southwest. Secondly, axial surfaces of anticlines which are commonly upright, have a more variable trend than those of the synclines (the poles along the primitive are mainly those of anticlinal axial surfaces).

(ii) The stereogram (Fig. 14) which is a composite of data from the north (Figs. 14 and 32), indicates a preferential dip of axial surfaces towards the east-northeast.

(iii) The areal configuration of axial traces in the south describes an arc with the convex side pointing towards the east-northeast (Figs. 1 and 13), whereas the data on Figs. 14 and 32 seem to describe an arc with the convex side pointing towards the west (Fig. 1). The isolated centres of no deformation at De Trap and De Bailie (Fig. 13) appear to be related to the associated divergent structural trends and cross-folding.

2.3 SECOND PERIOD OF PENECONTEMPORANEOUS DEFORMATION

2.3.1 *Introduction*

Small scale folding, well typified by magnitude and style, documents a second period of deformation. These phenomena were observed at De Trap, Groenberg and at Karookop (Fig. 32) where Visser (1962, 1965) followed by Rust (1967), described these structures as glacial grooves and striae.

At De Trap the deformation affected the Oskop Member of the Pakhuis Formation. Two stratigraphic horizons are similarly deformed at Karookop:

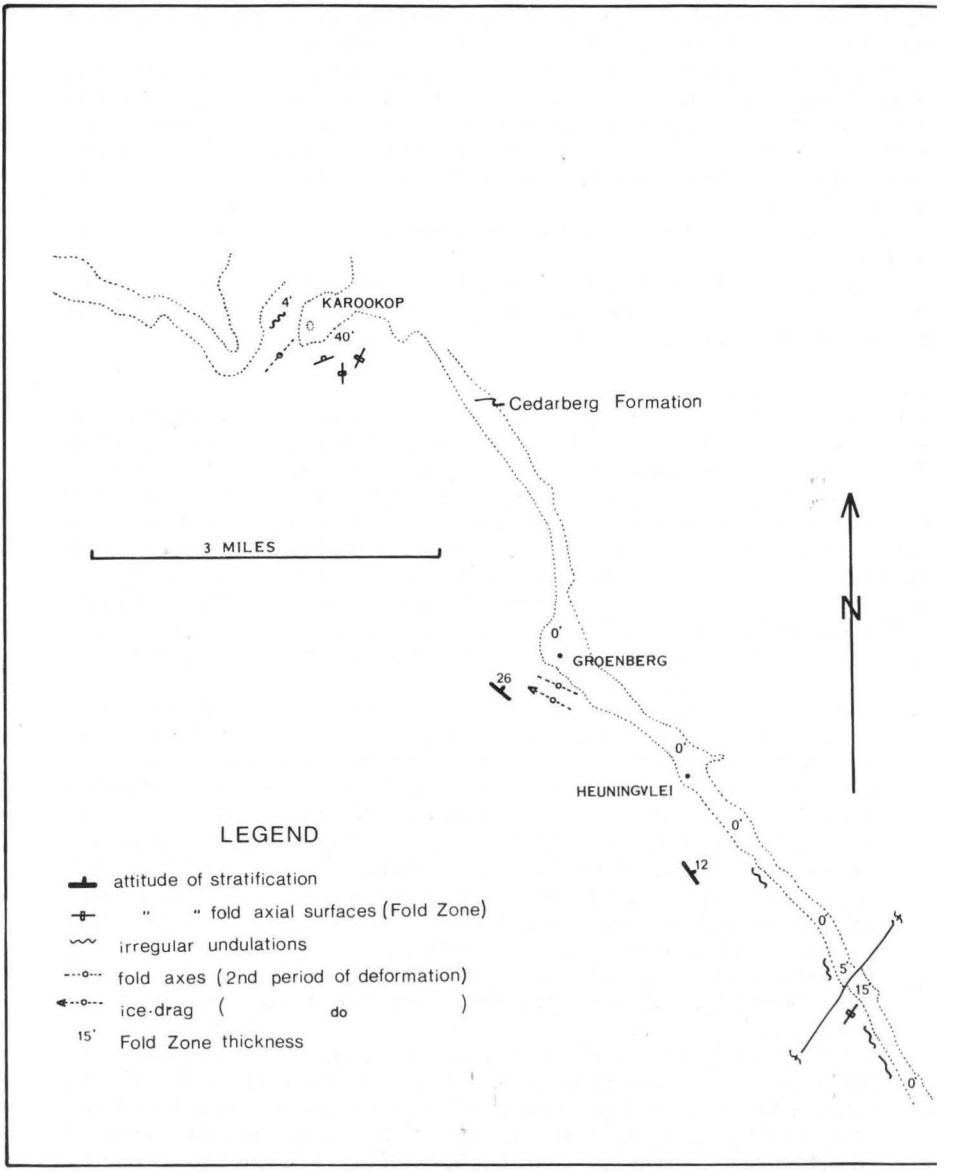

Fig. 32. Regional fold configuration and Fold Zone thickness southeast of Karookop.

(i) The uppermost unit of the Peninsula Formation (or Oskop Member after Rust, 1967 p. 43) which locally interfingers with overlying arenaceous diamictite.
(ii) An arenite lentil 1,8 m higher up in arenaceous diamictite (Kobe Member after Rust, 1967, p. 46).

2.3.2 *Structure*

Low irregular undulations (Plate XVII) in cross-stratified layers ($\lambda' = 6$ m $-$ 9 m, $2A = 1{,}2$ m $-$ 3 m) locally give way to cylindrical folding, notable for its regular spacing ($\lambda' = 60$ cm, $2A = 30$ cm) and rectilinear parallel trend of fold axes (Plate XVIII); symmetric and asymmetric forms were observed (Plates XIX and XX). Another feature of these folds is their periodical distribution (Plates XIX and XXI). Wrinkles are found only in the troughs of synclines.

At Karookop the depth of fold penetration in the cross-stratified layers is not known but the effect of folding on the underlying cross-laminae is clearly demonstrated by their sigmoidal posture on an eroded surface. At De Trap where the Oskop Member consists of sets of layers, both folding and wrinkling are penetrative within at least the upper 60 cm. The structural trends of the two periods of penecontemporaneous deformation correspond at least in the north (Fig. 32).

At Groenberg, on the upper surface of the Peninsula Formation, the same small scale folding is present in association with a grounded ice-block cast; Plate XXII illustrates an ice-thrust ridge (fold) which developed in front of the ice-block. Drag effects below the block are documented by linear drag marks and tools (first described by Rust, 1967 p. 76). Ripple marks can be seen beyond the ridge. The direction of movement of the ice block (probably caused by tidal currents) parallels the long axis of the small folds (Fig. 32), but is transverse to the ice-thrust ridge.

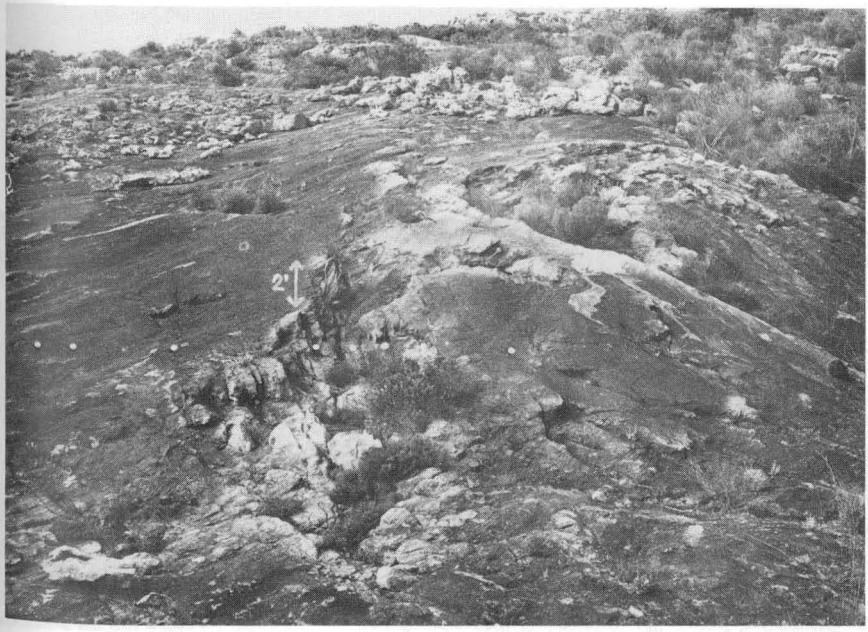

PLATE XVII
Irregular undulations in the upper surface of the Peninsula Formation (Karookop).

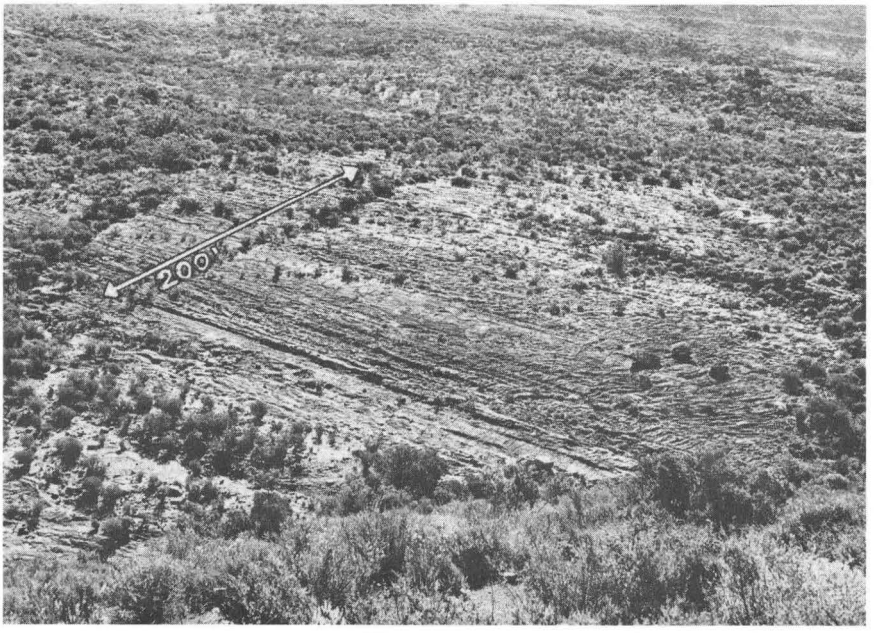

PLATE XVIII
A local occurrence of small rectilinear folds in the upper surface of the Peninsula Formation; note the regular spacing and parallelism (Karookop).

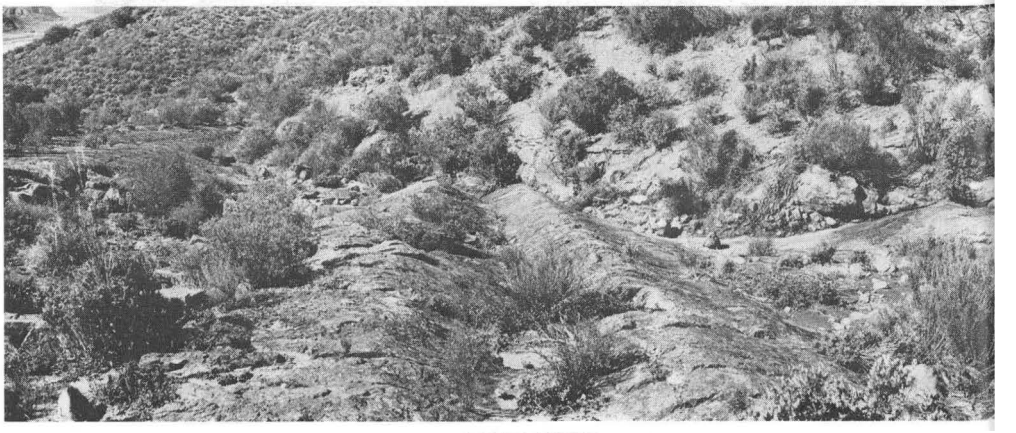

PLATE XIX
Rectilinear flutes underlying tillite (Karookop).

PLATE XX
An asymmetric flute (Karookop).

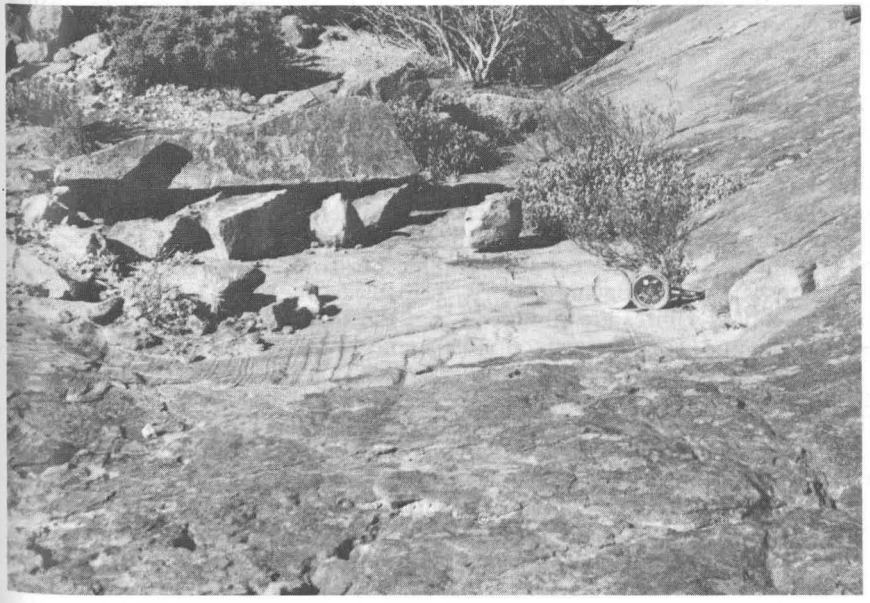

PLATE XXI
Fine wrinkles in the flute troughs (Karookop).

PLATE XXII
The cast of a grounded ice block on the upper surface of the Peninsula Formation; note the drag marks below and the ice-thrusted ridge in front (Groenberg).

3. INTERPRETATION

3.1 DEPOSITIONAL ENVIRONMENT OF THE GLACIOGENIC SEDIMENTS

Prior to the onset of glaciation a great thickness of cross-bedded Peninsula sands were deposited in the Table Mountain embayment (Fig. 2); relatively shallow water conditions are indicated (see Rust, 1967, for paleogeographical reconstruction). Subsequently an ice sheet invaded the depositional basin. The nature of the ice invasion is inferred from the rock record according to the principles set out by Carey and Ahmad (1961). Evidence for regionally spread subaqueous deposition during the terminal phases of each cycle (Table 3) further substantiates the depositional model of an ice shelf (grounded and floating) which advanced across a submerged embayment.

The rather peculiar nature of the arenaceous diamictites (tillites), occurring as they do at three different stratigraphic horizons, is central to the understanding of the glaciogenic history. The lower Sneeukop, upper Sneeukop and Steenbras Tillites are similar in that the rock is essentially a sandstone with a minor clastic matrix component and scattered clasts; the "stratification" as mentioned in the descriptive section consists of poorly defined undulating surfaces, not everywhere observable and not defined by sorting. These are unlike bedding structures normally associated with subaqueous deposition and might be the bounding surfaces of flow till units (This notion is further developed in Section 3.2). Where the arenaceous diamictite is more massive it might represent subglacial melt-out deposits. The arenite lentils which occur throughout are interpreted as the result of melt water action in the buoyancy line and/or englacial environments (cf. ice-contact-type structures microscopically observed). The sorted aspect of the arenaceous diamictite (being essentially a sandstone) without evidence of reworking by water is well explained by the idea of Rust (1967) that these diamictites represent

unconsolidated sands picked up by the ice sheet advancing across the marginal areas of the Table Mountain basin.

The regional persistence of the Oskop Sandstone, the unstratified character (in the normal sense) of the Steenbras Member, and the second period of ice-deformation necessitate two periods of ice advance and retreat (Table 3) to explain the observed succession of glaciogenic sediments (Fig. 33).

To allow for the formation of the Fold Zone, the first ice sheet advance must have been a grounded shelf depositing the lower Sneeukop sandy tills along the buoyancy line (therefore a wet-base ice sheet) and subsequently deforming it together with the upper Peninsula sand layers. The upper Sneeukop sandy tills represent retreating buoyancy line and subglacial melt-out tills and flow tills formed during the first retreat. These tills were reworked in part by a regional shore-line transgression giving rise to the thin Oskop sand sheet.

The second wet-base ice sheet advance was characterized by deformational features (the second period of deformation, Section 2.3) very unlike the large scale structures of the Fold Zone. The deformational features were developed on the upper surface of the Oskop Sandstone and lower horizons which were left unaffected by the first period of deformation. The structures at Groenberg are consistent with those formed by a grounded ice-block while the local development of flutings (cf. descriptions by Sugden & John, 1976, p. 237; Boulton, 1971) at De Trap and Karookop also indicate limited grounding of an ice mass.

As these deformational features are overlain by the Steenbras Member at De Trap and Karookop, and higher stratigraphic horizons at Groenberg, it is evident that at the onset of the second ice sheet advance, the ice shelf was only partly grounded; it became finally grounded to deposit the Steenbras sandy till subglacially and at the buoyancy line as a melt-out deposit. The second ice sheet retreat might have yielded more melt-out sandy till (conjecturally the upper portion of the Steenbras Member which is indistinguishable from the lower portion) and caused a major rise of the water level which lifted the remaining proximal part of the ice sheet and allowed for the ice-rafted deposition of the proximal Kobe stratified till; at this stage the floating ice shelf might have been polar.

The terminal sediments of the two depositional cycles (Table 3) differ in that the first cycle ends with a shallow water transgression whilst the deeper water conditions at the end of the last cycle are probably related to the larger

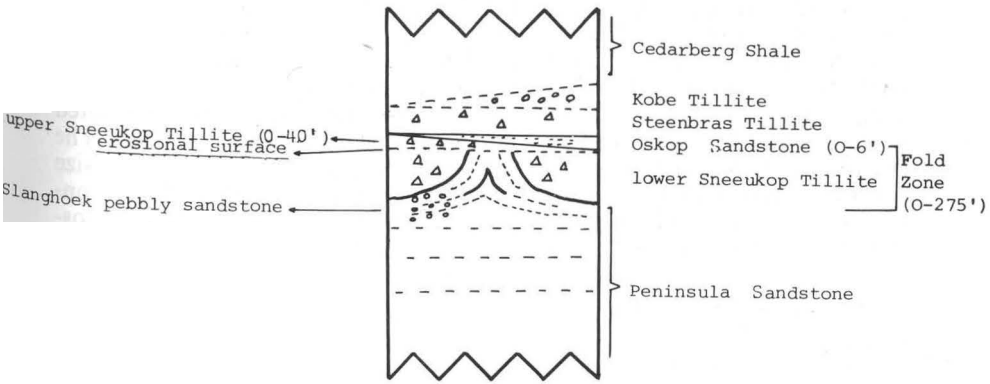

Fig. 33. Schematic stratigraphic column of the glaciogenic sediments as observed in the De Trap/Patryskop area. Refer to Table 3 for the sediment characteristics.

volumes of melting ice during the final retreat. It is interesting to note that the Table Mountain and Dwyka (Theron & Blignault, 1973) glaciations, both of which deposited sediments in active basins, gave rise to similar sediments (stratified clay-rich tillites grading into shale) during the final retreat.

A further difference between the two ice advances is the lack of significant deformation by the second advance. The possible reasons are (i) that the ice shelf was never fully grounded, (ii) that the underlying sediments were rendered competent by a large effective normal stress component. The first possibility is ruled out by the lack of proper stratification in the Steenbras Member. It is concluded therefore that the second ice advance constituted a thicker ice sheet and/or took place under less buoyant conditions than the first advance.

3.2 PALEOCURRENT DATA

The directional observations (Section 2.3) on the second ice sheet advance (i.e. the flutings and grounded ice block features), are not consistent; their paucity does not warrant further interpretation.

The microfabric results from the lower Sneeukop Member which forms part of the Fold Zone have to be considered with regard to the deformation. Some samples, however, yielded three-dimensional microfabric patterns (see discussion in Section 2.1.4.2) symmetrical with respect to the depositional interface as observed from nearby arenite lentils, and resemble simple primary microfabric patterns of undeformed sediments. It is thought that these hand-sized samples represent largely unstrained domains. The large angle, but non-orthogonal relation between the two principal modes on the ab(Sed.)-surface and absolute values of imbrication angles, however, might be a function of the strain imposed by the glacial folding. One sample is totally asymmetric, probably as a result of the deformation. The consistency of the vectorial results from the lower Sneeukop arenaceous diamictite further substantiates the interpretation above; primary flow directions of the transport medium (Figs. 5D, 7A and B, Map 2) are 126°, 170° and 160° and differ largely from the ice-sheet flow direction ($\pm$080°) as inferred from the Fold Zone structure. This discrepancy together with the different modes of transport indicating a variable flow regime (Section 2.1.4.2) for the transport medium of the sandy till, show that at least part of the sandy till was transported after deposition from the ice sheet. The lack of stratification and presence of a wacke-type matrix material in the arenaceous diamictites eliminates water reworking; high density turbulent liquid flows or more plastic mass flows in front of the buoyancy line are considered the more likely redistribution transport media of the sandy tills.

A macrofabric analysis of the upper Sneeukop Member at De Trap yields a flow direction of 172° (Fig. 9) and is consistent with the results from the lower Sneeukop Member; this trend also corresponds to the regional flow trend reported by Rust (1967). The three-dimensional aspect of the microfabric patterns from the upper Sneeukop Member cannot be interpreted due to a $\pm$10° dip uncertainty with respect to the depositional interface. The differential constraint imposed on the orientation of grains of different size fractions on the apparent ($\pm$10°)ab(Sed.) – surface, agrees with fluid-flow conditions (see discussion in Section 2.1.4.3) of perhaps liquid flow tills as opposed to more viscous mass flows (cf. Boulton, 1971, p. 50).

3.3 RHEOLOGY OF THE SEDIMENTS DURING DEFORMATION

3.3.1 *Peninsula arenite*

The absence of erosional features such as unconformities, channels, and fossil soil profiles at the arenite/diamictite interface (Rust, 1967) indicates that deposition of the Peninsula sand was followed uninterruptedly by the de-

TABLE 3

THE GLACIOGENIC SEDIMENTS OF THE TABLE MOUNTAIN GROUP AND THEIR MODE OF DEPOSITION

Stratigraphic unit	Lithologic characteristics	Depositional aspect	Ice advance
Kobe Tillite	Varies from pebbly mudstone to clay-rich stratified diamictite with outsize and rafted clasts	Ice rafted from floating ice shelf	Second cycle
	(interlayered gradational contact)		
Steenbras Tillite	Arenaceous diamictite (i.e. arenite with interstitial clay material and scattered rudite clasts) similar to the Sneeukop diamictite	Subglacial and advancing buoyancy line melt-out till and perhaps flow till	
	(mostly sharp contact)		
Oskop Sandstone	Single or multiple cross-stratified zone; regionally persistent, but locally discontinuous; very sparse erosion channels in pre-Oskop surface	Blanket transgression	First cycle
	(sharp or interlaminated gradational contact)		
Upper Sneeukop Tillite	Arenaceous diamictite	Subglacial and retreating buoyancy line melt-out till and flow till	
	(erosional surface)		
Lower Sneeukop Tillite	Arenaceous diamictite; deformed	Advancing buoyancy line melt-out deposit and flow till	
	(sharp contact)		
Slanghoek pebbly sandstone ..	Pebble-rich sandstone developed in discontinuous fashion	Proglacial channel fill	

position of the Sneeukop diamictites. An unconsolidated condition for the Peninsula sand during deformation is implied.

The mode of transposition and conservation of structure during folding imply hydroplastic behaviour of the sand (Elliot, 1965). Sparse examples of rupture indicate solid or quasi-solid behaviour, which was effective after hydroplastic transposition. Apparently the hydroplastic strain limit was exceeded under local conditions of tensional stress (Fig. 4H).

3.3.2 *Lower Sneeukop diamictite*

Microfabric analysis of samples taken approximately in the central part of the Member reveals typical primary textures. The preservation of primary textures rules out the possibility of liquid or quasi-liquid behaviour (Elliot, 1965) at least for this horizon.

The sedimentary dikes always lie in the ac(Geom.)-plane of the synclines, indicating that dike formation was contemporaneous with, and controlled by the deformation. Solid tensional fracturing preceded injection of the dike material. The implication is that a large part of the lower Sneeukop Member behaved as a solid while portions, the source of the injected diamict, was in quasi-liquid state. Quasi-liquid behaviour of the diamict in the dikes is indicated by grading within the dikes; the central part of the dike constituted the more competent flow regime.

S_3-surfaces, infrequently found at or near the diamictite/Peninsula arenite contact, represent discrete slip surfaces which are more likely to be formed in a hydroplastic than quasi-liquid sediment.

Solid/quasi-solid behaviour of the basal part of the diamict is ruled out by the occurrence therein of detached bands of Peninsula arenite. During an "advanced" stage of deformation (i.e. after transposition took place) S_3- and/or S_4-bands became parted from the Peninsula sand contact by a splaying mechanism. Progressive deformation, in some instances, further folded and buckled these S_3- and/or S_4-bands. Whereas both the Peninsula sand and the diamict near the contact are considered to have been in a hydroplastic state, their relative competency is clearly illustrated by the fact that the sand behaved as an entity while the diamict flowed in a more unconstrained manner.

The same relation is illustrated where clasts are partly embedded in the Peninsula arenite. A certain amount of relative slip during flexural-slip folding is expected on the contact surface. As no relative movement between the clasts and arenite is evident, it is inferred that the flowing diamict exerted little pressure on the obstructive clasts.

3.3.3 *Discussion*

The behaviour of unconsolidated sediments under stress can largely be inferred from the Mohr-Coulomb law (Matthews and MacKay, 1960; Williams, 1960; Viete, 1960; De Sitter, 1956):

$\tau(\text{crit}) = \tau o + (\sigma - p) \tan \phi$

where the critical shear stress τ(crit) is a function of

(i) the cohesion of the sediment (τo),
(ii) the total normal stress (σ),
(iii) the hydrostatic pore pressure (p) and
(iv) the angle of internal friction (ϕ).

Cohesion, pore pressure and internal friction (shearing resistance) are functions of grain size and grain size distribution. Cohesion increases with a decrease in grain size and approaches zero for sand. The angle of internal friction is ca. zero for saturated clays and 30° — 35° for sand (Spencer, 1969). Pore pressure controls effective stress (σ — p) which is partly dependent on the density of the sediment in relation to its critical density (De Sitter). The effect of pore pressure is largely dependent on permeability and rate of stress application; thus a clay would be more easily liquified than a sand.

The sedimentary environment of the Table Mountain Group suggests a water saturated condition of the sediments prior to deformation. Theoretical considerations indicate that the Peninsula sand would have required a relatively large critical shearing stress. This appreciable shearing stress could be reduced by increased pore pressure and/or by the observed adjustment along potential slip surfaces, such as S_1 and S_2 (rotation/transposition, Section 2.2.4).

The total absence of thrust faulting is significant (by comparison with similarly deformed sediments – Section 3.4) and may in part express this mode of stress accommodation. The permeability of the sand, coupled with a not too rapid application of stress, would have inhibited the local development of high pore pressures which facilitates thrust faulting. The development of the Fold Zone structures indicates optimum normal stress conditions allowing the plastic deformation of the sand but not rendering the critical shear stress of the sands large enough to inhibit deformation. This condition relates to the effective load of the ice sheet which again is a function of the ice-sheet thickness and the counteracting buoyancy conditions.

A relatively low critical shearing stress for the lower Sneeukop diamict can be inferred from its bad sorting (low permeability) and notable clay content. The homogeneity of the diamictite lithosome contrasts sharply with its inferred variable rheologic behaviour during deformation. The general plastic behaviour and solid tensile fracturing of the diamict express the different behaviour of material under shearing and tensile stresses respectively. The interstitial clay material of the diamict should increase pore pressure under the stress and the blanketing effect of an overriding ice sheet, with the result that the diamict should behave more incompetently than the Peninsula sand and becomes locally liquified to produce the dikes. At the diamict/sand interface, the more permeable Peninsula sand drained off pore water in the diamict, thereby increasing its critical shearing stress and allowing S_3-slip surfaces to develop in it.

In Section 2.2.4 it is demonstrated that the quartz grain long axes of the folded Peninsula sand define a new, imposed subfabric. The near perfect development of the new subfabric relates both to the amount of shear strain and the conditions which allowed for the degree of mechanical reorientation.

3.4 REVIEW OF PLEISTOCENE ICE-DEFORMATIONAL FEATURES

One avenue of approach to explain the processes of Paleozoic ice-deformation is to consider the knowledge gained elsewhere where models are constrained by more and better data.

The directional aspects of Pleistocene ice-sheet movement in the northern hemisphere are known from observations independent of associated deformational features.

The deformation of unconsolidated substrata by overrriding ice-sheets and glaciers of Pleistocene age has been described by Fuller (1914), Slater (1926, 1927), Byers (1959), Viete (1960), Kupsch (1962), Rutten (1960, 1965), Mathews and MacKay (1960, 1964, 1965), and Dellwig and Baldwin (1965). The main features are listed below.

1. Mainly compressional structures develop while tensional forms are rare. The *larger structures* are usually folds and thrust faults. Folds with a vertical extent of 150 m-180 m and thrust faults with dip-slip components of 45 m-60 m have been reported. Ice-thrust ridges are characteristically sharp-crested; bevelling of the folds may be due to flowing ice. Synclines are generally much wider, their axes being 50 m-100 m apart. Fold axes commonly converge along strike and thrust planes show slickensides and grooves. Allochtonous rafts (locally a few km across), having been incorporated as englacial material, undergo deformation in the same

manner as the glacial ice itself; some are broken into fragments and deposited with an imbricate structure.

2. The following *small structures* have been described:
   (*a*) Minor folds.
   (*b*) Sedimentary dikes which tend to be sub-parallel with the normal to the ice-front.
   (*c*) Irregular intrusions i.e. mutual flow effects between beds; mixing of rotated slabs of material from a lower bed with the overlying material.
   (*d*) Fuller (1914; Fig. 140) shows an irregular contact where the bottom material is splayed along bedding planes.
3. *Deformational zones*, characterized by different types of structures, can be related to distance behind the ice-front; imbricate thrust blocks form closest to the terminus whilst flat lying folds originate further back by frictional drag underneath the ice mass.
4. The folds form *transversely* to the direction of ice-flow. Axial planes and thrust faults usually dip in a direction opposite to ice-flow. The plunge of individual fold axes may range from 20° to 35° in opposing directions; thus several culminations and depressions appear on strike within the same fold. Structural features typically define an arcuate pattern in plan, with the convex side pointing in the direction of ice-flow.
5. The relation between the deformed structures and the *overlying till* is well described by Kupsch (1962): "The ablation till lies disconformably on the bevelled bedrock structures, but the basal till constitutes a conformable part of the deformations".
6. The absence of *inverted fold limbs* in association with thrust faults indicates superficial folding (De Sitter, 1956; p 405) and disproves gravitational gliding (De Sitter, 1964; p. 255).
7. *Controlling factors* of deformation are firstly the nature of the overridden sediment and secondly the static and dynamic pressures exerted by the ice-load. These are functions mainly of ice thickness, velocity of flow and topography.
   (*a*) Kupsch estimated that *ice thicknesses* of 140 m-280 m formed ice-thrust ridges with 60 m vertical dimension. According to Viete (from Kupsch): ". . . the static pressure exerted by a glacier 200 m thick varies between 18 kg/cm² for clean ice to as high as 36 kg/cm² for ice choked in debris". Huizinga (1944; from Kupsch) pointed out that a minimal lateral push of ca. 300 kg/cm² is necessary to form ice-thrust ridges. Kamb (1964) regards the shearing stress at the bottom of glaciers to be roughly constant at 1 kg/cm². ". . ., there is considerable evidence to support the view that deformation commonly occurred near the margin of an actively moving lobe" (Matthews and MacKay, 1960). Kupsch explains: "It has been observed in existing glaciers that thrusting in ice is best developed near its margin, where the rigid upper surface of the glacier, which further upstream overlies plastic ice, extends to the base . . ."
   (*b*) Pre-glacial topography is an important controlling factor; the maximum development of structures is along slopes facing the direction of ice-flow and along borders of pre-glacial valleys. Mathews and MacKay (1964) do not consider an opposing slope a necessary condition for ice-thrusting.
   (*c*) Controversial opinions have been expressed by Kupsch and Mathews and MacKay (amongst others) on the effect of ground-ice on ice-thrusting. Mathews and MacKay (1960) conclude that:
      (i) The shear strength of sediments usually exceeds the shear stress applied by a glacier on its substratum (1 kg/cm²). "Abnormal circumstances such as unusually high shear stress beneath the ice, unusually low shear strength of soils, or unusually high pore

pressures seem, however, to have permitted shear failure in many widely separated localities".

(ii) The development of interstitial ground-ice is not a necessary condition to transmit stress as loading by the overlying ice would render the sediments sufficiently competent.

8. Various modes of deformation by the overrriding ice have been postulated:
   (*a*) Incorporation of substratal material by the glacial ice will result in a glacial pseudomorph structure of such material.
   (*b*) Ice-push in front of the ice sheet.
   (*c*) Frictional drag beneath the ice-sheet by means of a basal slip mechanism.
   (*d*) A permafrost substratal layer in essence constitutes part of the glacier and becomes deformed by glacier tectonics.

3.5 ICE SHEET DEFORMATION IN THE FOLD ZONE

3.5.1 *A priori considerations*

The intraformational nature of the Fold Zone, *per se*, with respect to a glaciogenic stratigraphy is well established and its contemporaneous formation due to subglacial deformation is furthermore assumed. A comparison of Pleistocene glaciotectonic features (reviewed in the previous section) with the structure of the Fold Zone (Section 2.2), reveals strong similarities. It is therefore deduced that the ice movement inferred from the domainally consistent fold vergence and arcuate pattern in plan, is as shown in Fig. 1. Dissimilarities may indicate more specific conditions, for instance the apparent absence of allochtonous rafts points to either wet-base ice sheets and/or the absence of localized high pore pressures (see discussion of Moran, 1971 and Banham, 1975).

3.5.2 *External geometry and ice flow*

The relation between the embayment axis and external geometry of the Fold Zone (Fig. 2), especially the gradual decrease in Fold Zone thickness towards the embayment margin, indicates a regionally operating force markedly affected by the basin shape. Both on theoretical (Boulton, 1975) and observational (Pleistocene model) grounds it is known that deformation of unlithified subglacial sediments increases towards the outer margins of ice sheets because of the lower critical shear stress due to decreased effective loads. The contours depicting the Fold Zone thickness in Fig. 2 can therefore be regarded as parallel to an ice sheet front encroaching on an embayment (Fig. 36, stage 1); the flow lines being normal to the ice front, converge towards the open end of the embayment. The flow lines thus deduced, essentially correspond with the pattern of ice flow inferred from structure (Fig. 1).

3.5.3 *Isolated centres of no deformation and interference folding*

The isolated centres of no deformation situated in areas where the deformation otherwise persists can be ascribed to the following:

(i) Local floating of the ice shelf (low areas).

(ii) Locally less buoyant conditions or a thicker ice shelf (high areas).

Apart from the unlikely condition that an ice shelf varies considerably in thickness over distances of say 2 km the other possibilities relate to an uneven subglacial topography.

The further possibility that the interference folding and deviatory fold trends at De Trap and De Bailie (Fig. 13) might be related to the domains of no deformation, lead to the conclusion that these domains represented competent areas causing deviations from the regional fold pattern; if this observation can be substantiated by further investigation, the isolated centres of no deformation would be ascribed to a positive subglacial topography. An alternative but not virtually exclusive explanation for the interference

folding and deviatory trends, may be sought in the radial expansion advance mechanism of ice sheets (see also Section 3.5.7).

3.5.4 *Fold zone boundaries*

The regularity of the lower bounding surface of the Fold Zone, as viewed from a distance, indicates a non-variable stress application as would be expected from an ice sheet of uniform thickness. The décollement along the lower boundary is due to local adjustment to accommodate the concentric folding; large scale displacement was never observed and relates to the rheological properties of the homogeneous Peninsula sand (Section 3.3.3).

The upper boundary constitutes an erosional unconformity which, according to the depositional model set out in Section 3.1, implies that the advancing grounded ice shelf deformed and eroded the underlying sands and tills in the wake of the buoyancy line. Thus the Peninsula sand, at least in part, formed the provenance of the Sneeukop sandy tills.

3.5.5 *Deformation*

To explain the mechanics of folding in terms of an overriding ice sheet, the Fold Zone structures have to be considered.

3.5.5.1 Simple shear

The rotation of fold axial traces (in profile) towards parallellism with the upper boundary of the Fold Zone (Fig. 12), indicates a simple shear deformation system (cf. Ramsay, 1967; Ramsay and Graham, 1970) with the upper boundary of the Fold Zone situated towards or at the core of the shear zone. This interpretation is also consistent with the Pleistocene ice-deformational features (Section 3.4) and the depositional model (Section 3.1) which invokes an overriding ice sheet. In terms of both the Pleistocene model and shear zone kinematics, the fold vergence indicates the same sense of ice sheet movement.

3.5.5.2 Upright folding

The simple shear model does not explain all the features of the Fold Zone.

Symmetric upright folds (Sections 2.2.2 and 2.2.6) predominate towards the proximal margin of the Fold Zone. Judging from (i) the concentric folding dying out downwards, (ii) decrease in interlimb angle upwards, (iii) increase in rotation/transposition upwards and (iv) occurrence of subsimilar fold forms higher-up, the Fold Zone constitutes a domain of heterogeneous strain with a regular increase of strain upwards. These effects are also observed where overfolding is developed and were probably enhanced by the simple shear deformation. The overfolding always turns into upright attitudes towards the bottom part of the Fold Zone (Fig. 12).

The regional pattern is therefore one of upright folding developed throughout, with overfolding of the upright folds towards the distal part of the embayment. As the simple shear model (Ramsay, 1967; Ramsay and Graham, 1970) does not allow for axial traces to be orientated normal to the shear trend (as seen in the ac-section), the symmetrical upright folding has to be accounted for by an alternative model.

Coward (1976) showed that the strain distribution across a shear zone of short finite length cannot be explained by simple shear alone. He concluded that shear zones with a high rate of displacement relative to rate of propagation, develop a phase of pure shear at the leading edge which is later superimposed by simple shear deformation. According to this shear model of Coward then, layer parallel shortening could have resulted in the formation of the upright folds which were subsequently rotated by simple shearing.

As all the structural features (apart from the rotation) which developed in the overfold domain are also observed in the upright fold domain, it is

conjectured that the upright folding constitutes the major fold event and contributed to the bulk of the finite strain, whereas the simple shear event resulted mainly in the rotation of the fold axial surfaces and development of the erosional angular unconformity at the top of the Fold Zone.

3.5.5.3 Bulk strain ellipsoids

The XY-plane ($X > Y > Z$, the principal finite elongation directions of the strain ellipsoid) is considered to be orientated along the axial planes of the folds. The pod folds and characteristic development of culminations and depressions during the upright folding event indicate shortening along the Y-axis as well; the resultant bulk strain ellipsoid is therefore of the constrictional type ($X > 1 > Y > Z$) with the XY-plane in a subperpendicular attitude and Y statistically subparallel to the fold axes. During the later simple shear event (Section 2.2.3.2) sedimentary dikes formed normal to Y (the dikes are never folded and therefore formed late during the folding) and indicate extension along the Y-axis; the bulk strain ellipsoid is of the flattening type ($X \geq Y > 1 > Z$)* with Y statistically subparallel to the fold axes and the XY-plane regularly variable such that towards the upper boundary of the Fold Zone XY tends tangentially towards parallelism. The association of the flattening-type bulk strain ellipsoid with the simple shear event, is based on observations from the De Trap/Patryskop area (Fig. 13); it is not known whether this association is regionally persistent.

3.5.6 *Fold development*

(i) The initial layer parallel shortening gave rise to the typical folded forms as illustrated in Fig. 34 and also allows for the simultaneous buckling of the ice/sediment contact. The cusps point upwards and show that the overlying ice behaved more competently than the sediment (cf. Ramsay, 1967, p. 383); the lower portion of an ice sheet can be rendered relatively competent by a sediment load while the demonstrated ability of the Peninsula sand to accommodate strain by layer boundary slip and cross-bedding rotation, allows it to behave relatively incompetently.

(ii) The strain distribution in the folded layers (Fig. 34) is based on the qualitative observation of layer thickness, the amount of rotation/transposition of the cross-bedding and the geometry of the rotation/transposition process (Section 2.2.4). The anticlines formed by flexural-slip which, in the upper attenuated parts, was accompanied by a significant amount of flattening strain. The attenuated form of folded layers along the outer arc of the synclinal hinges, indicates internal deformation by tangential longitudinal strain (terminology after Ramsay, 1967); the thickening of the lower Sneeukop Member along the inner arc is predicted according to the tangential longitudinal mode of strain accommodation in the synclines.

(iii) By measuring along the length of folded layers, the amount of shortening is calculated at 47% ($n = 4$); shortening in the upper part of an attenuated anticlinal hinge amounts to 72% (the effects of pre-buckle layer thickening and post-buckle flattening were disregarded in the strain determinations). In view of the constrictional type of bulk strain ellipsoid inferred for the layer parallel shortening event and assuming no volume change, it is concluded that the extension along the vertical (X-axis) was at least 50% in the De Trap/Patryskop area.

*In designating relative magnitudes to the principal strain axes with respect to the initial unit sphere, the possibility of volume change is not considered.

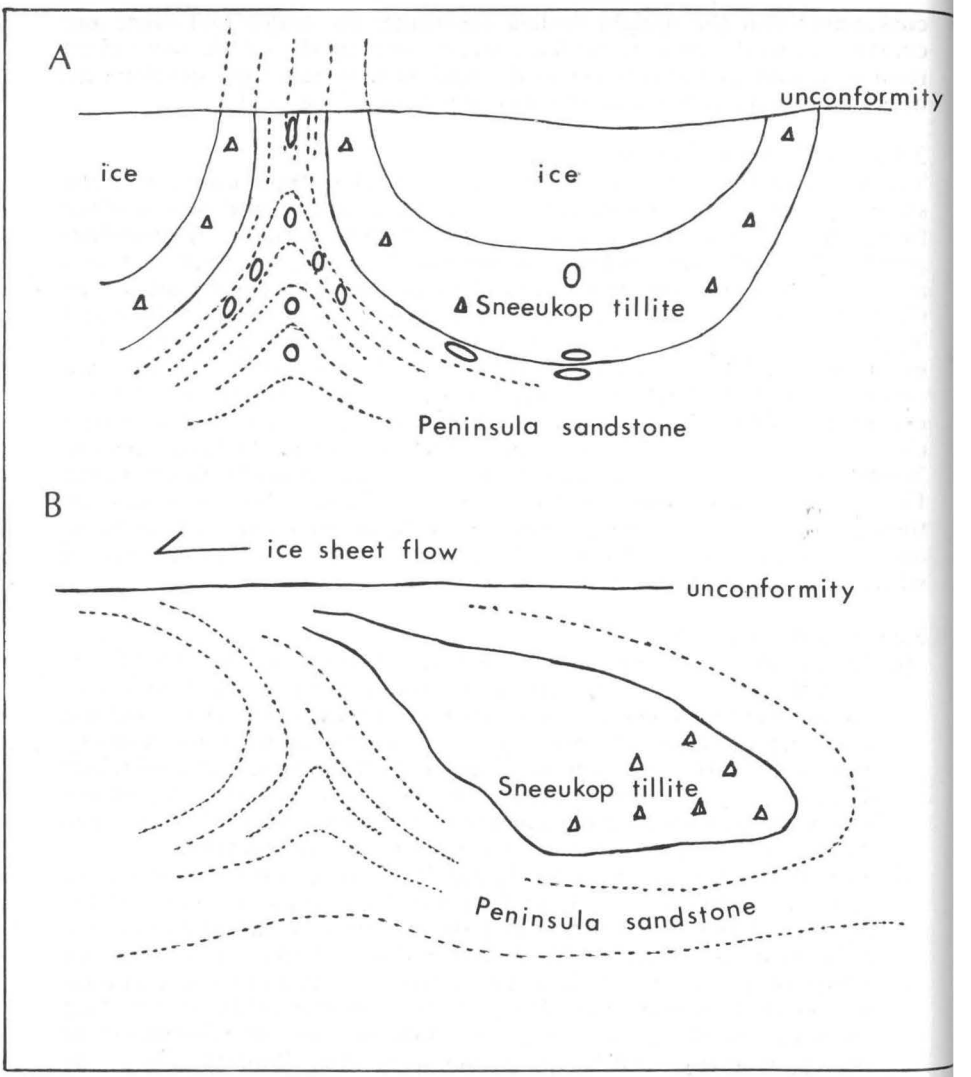

Fig. 34. A schematic presentation of the fold development. A. Upright buckling by the initial layer parallel shortening event during compressive ice flow without a significant amount of basal slip; the strain distribution is indicated by the ellipses. B. The subsequent simple shear event during basal slip caused rotation and development of elasticas by ice melting in the synclinal cores.

(iv) The simple shear event rotated the axial surfaces (Fig. 34). At this stage the overturned synclines would be cored by the lower part of the ice sheet which, when subsequently melted, would explain the formation of the elasticas.

(v) Both on a local and a regional basis in the De Trap/Patryskop area, the fold axes preferentially plunge 7° in a direction 330°. This could mean that the depositional interface had a 7° slope towards the north-north-west prior to deformation; this explanation is rejected on the grounds that a 7° slope is too steep and that the dip is towards the proximal side

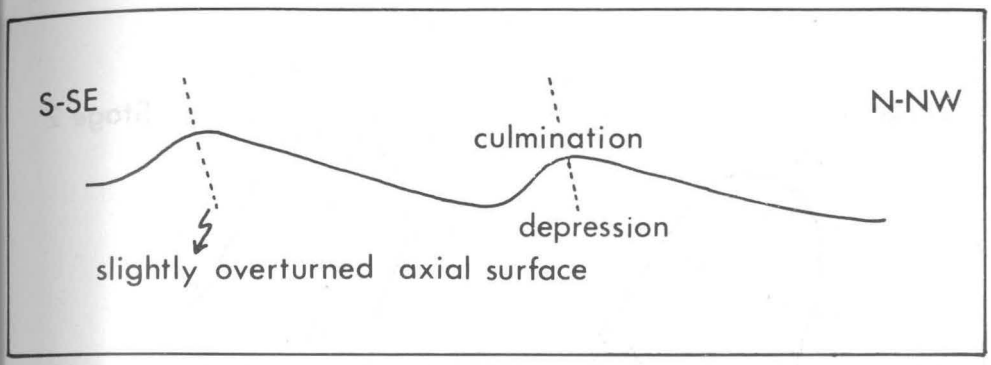

Fig. 35. A schematic longitudinal section of a non-cylindrical fold showing the inferred asymmetry.

of the embayment. Alternatively, the preferential north-northwesterly plunge is considered to reflect the asymmetric profiles of longitudinal sections through the non-cylindrical folds (Fig. 35); areally-wise random samples would be located preferentially on the long and shallower north-northwesterly limbs. The attitude of a constrictional bulk strain ellipsoid which represents the layer parallel shortening event operating along the depositional interface does not explain the slight rotation necessary to provide the asymmetric longitudinal profiles; therefore another simple shear event of low magnitude is invoked to explain the slight rotation towards the south-southeast.

3.5.7 *Ice flow*

The structural analysis of the Fold Zone leads to the conclusion that the structure can be explained in terms of three deformation processes:

(i) The initial layer parallel shortening or pure shear event with a resultant constrictional bulk strain ellipsoid with Y subparallel to the embayment axis.

(ii) A subsequent simple shear event with an associated flattening-type bulk strain ellipsoid (Y subparallel to the embayment axis).

(iii) Another simple shear event of low magnitude and directional parameters subparallel to the embayment axis (and probably post-dating (i)).

These different deformation events are interpreted as part and parcel of one ice flow process i.e. the progressive infill of the Table Mountain embayment (Fig. 36). Nye (1952) distinguished between two types of glacier flow viz. compressive and extending flow. According to the model of Coward (1976) a component of pure shear develops in shear zones when the rate of shear strain is high relative to the rate of propagation of the shear zone; as these are more or less the conditions under which Nye's compressive flow develops, one can relate compressive flow to pure shear deformation and also extending flow to simple shear deformation.

The movement path of a grounded ice shelf into the Table Mountain embayment is reconstructed according to the structural development of the Fold Zone (Fig. 36).

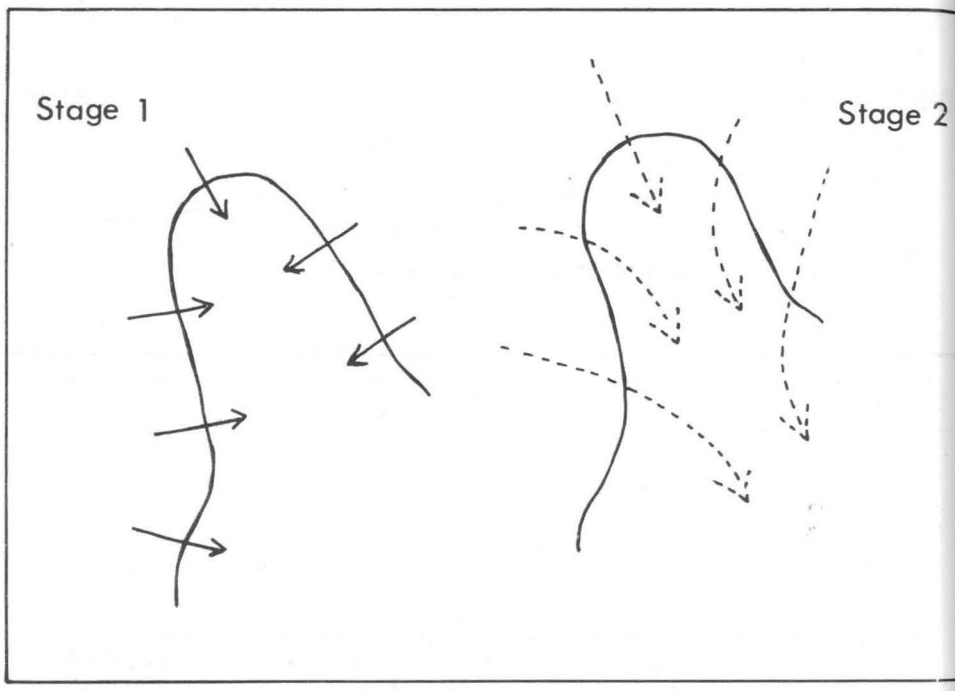

Fig. 36. The initial and mature stages of an ice sheet advancing into the Table Mountain embayment.

Stage 1

The grounded ice-shelf advance continued until opposing shelves met and pronounced compressive strain/flow without basal slip developed, causing the upright folding event. The constrictional bulk strain ellipsoid is considered a reflection of compressive strain due to the end-on infill of the embayment. The minimum of 50% stretching along the vertical in the deformed sediments would give an indication of the amount of ice sheet thickening at this stage if the bulk strain was operative throughout the whole thickness of the ice sheet. The first layer parallel shortening event is considered the major deformation event, causing the bulk of the structural features designated as the Fold Zone; the schematic ice flow pattern (Fig 36, stage 1) is therefore constructed in accordance with the ice flow pattern inferred from the external geometry of the Fold Zone (Section 3.5.2).

During the initial stages of the ice shelf advance prior to the development of compressive flow, buckling by simple shear was not possible because the sand layers were orientated subparallel to the direction of no infinitesimal longitudinal strain (also the shear direction of basal slip).

The subsequent simple shear event, associated with the erosional unconformity, is ascribed to renewed basal slip which affected the rotation of the previously formed axial surfaces. The renewed basal slip developed at the onset of stage 2 (Fig. 36) when pronounced extending flow developed towards the open end of the embayment.

The basal slip, as indicated by the sense of rotation, continued in the same direction as the initial advance. Pronounced effects of basal slip

were only observed towards the distal part of the embayment where the effective load had not yet rendered the sediments too competent to deform. The observation of an erosional unconformity in association with upright folds (Fig. 34) demonstrates that, although basal slip operated, the sediments in some domains were too competent to deform.

Stage 2

It is possible that the interference structures, observed at De Trap, developed during the transition from stage 1 to stage 2.

The expected flow pattern (Fig. 36) during this more mature stage of ice infill, is thought to be reflected by the preferential north-northwesterly dip of fold axes (discussion in Section 3.5.6(v)) which is interpreted as the result of a simple shear event with basal shearing towards the south-southeast. The increased effective load pressure in the De Trap/Patryskop area at this stage, was such that this simple shear event only had a minor effect on the now competent Peninsula sands. This is also the reason why the Fold Zone geometry and structures reflect the initial ice flow pattern and not the mature stage (Fig. 36).

ACKNOWLEDGEMENT

The guidance of Prof. I. C. Rust is gratefully acknowledged.

REFERENCES

American Commission on Stratigraphic Nomenclature (1961). Code of stratigraphic nomenclature. *Bull. Am. Ass. Petrol. Geol.*, **45**, 645-665.

Badgley, P. C. (1965). Structural and tectonic principles. Harper & Row, New York, 521 pp.

Banham, P. H. (1975). Glacitectonic structures: a general discussion with particular reference to the contorted drift of Norfolk, 69-94. *In* Wright, A. E. and Moseley, F., Eds., *Ice ages: ancient and modern.* Geological Journal Special Issue, No. 6. Seel House Press, Liverpool, 320 pp.

Bhattacharyya, D. S. (1966). Orientation of mineral lineation along the flow direction in rocks. *Tectonophysics*, **3**, 29-33.

Blignault, H. J. (1970). *Contemporaneous glacial folding in the Table Mountain Group, Western Cape.* M.Sc. thesis (unpubl.), Univ. Stellenbosch, 41 pp.

Boulton, G. S. (1971). Till genesis and fabric in Svalbard, Spitsbergen. *In* Goldthwait, R. P., Ed., *Till: a symposium.* Ohio State University Press, 402 pp.

Boulton, G. S. (1972). Modern Arctic glaciers as depositional models for former ice sheets. *J. geol. Soc.*, **128**, 361-393.

Boulton, G. S. (1975). Processes and patterns of subglacial sedimentation: a theoretical approach, 7-42. *In* Wright, A. E. and Moseley, F., Eds., *Ice ages: ancient and modern.* Geological Journal Special Issue, No. 6. Seel House Press, Liverpool, 320 pp.

Byers, A. R. (1959). Deformation of the Whitemud and Eastend Formations near Claybank, Saskatchewan. *Trans. R. Soc. Can.*, **53**, Ser. 3, Sect. 4, 1-11.

Carey, S. W. and Ahmad, N. (1961). Glacial marine sedimentation. *Proc. 1st Int. Symp. on Arctic Geology*, 2. University of Toronto Press, Toronto, 1 196 pp.

Cocks, L. R. M., Brunton, C. H. C., Rowell, A. J., and Rust, I. C. (1969). The first Lower Palaeozoic Fauna proved from South Africa. *Q. J. geol. Soc. Lond.*, **125**, 583-603.

Coward, M. P. (1976). Strain within ductile shear zones. *Tectonophysics*, **34**, 181-197.

Dellwig, L. F. and Baldwin, A. D. (1965). Ice-push deformation in northeastern Kansas. *Bull. State geol. Surv. Kansas*, **175** (2).

De Sitter, L. U. (1956). Structural geology. McGraw-Hill, New York, 552 pp.

De Sitter, L. U. (1964). Structural geology. McGraw-Hill, New York, 551 pp.

Elliot, R. E. (1965). A classification of subaqueous sedimentary structures based on rheological and kinematical parameters. *Sedimentology*, **5**. 193-209.

Evenson, E. B. (1971). The relationship of macro- and microfabric of till and the genesis of glacial landforms in Jefferson County, Wisconsin. *In* Goldthwait, R. P., Ed., *Till: a symposium.* Ohio State University Press, 402 pp.

Fleuty, M. J. (1964). The description of folds. *Proc. geol. Ass.*, **75**, 461-492.

Flint, R. F., Sanders, J. E., and Rodgers, J. (1960a). Symmictite: a name for nonsorted terrigenous sedimentary rocks that contain a wide range of particle sizes. *Bull. geol. Soc. Am.*, **71**, 507-510.

Flint, R. F., Sanders, J. E., and Rodgers, J. (1960b). Diamictite: a substitute term for symmictite. *Bull. geol. Soc. Am.*, **71,** 1809-1810.
Fuller, M. L. (1914). The geology of Long Island, New York. *Prof. Pap. geol. Surv. U.S.*, **82.**
Haughton, S. H. (1929). The glacial beds in the Table Mountain Series. *Int. geol. Congress Rep. 15th Sess.*, S. Afr. 1929, Pt. II, 85-89.
Haughton, S. H., Krige, L. J., and Krige, A. V. (1925). On intraformational folding connected with the glacial bed in Table Mountain Sandstone. *Proc. geol. Soc. S. Afr.*, **28,** 19-25.
Huizinga, T. K. (1944). Geologie en grondmechanica. *Geol. Mijnbouwk. Genoot. Ned. en Koloniën*, Geol. Ser., **14,** 259-275.
Kamb, B. (1964). Glacier geophysics. *Science*, **146,** 353-365.
Kupsch, W. O. (1962). Ice-thrust ridges in western Canada. *J. Geol.*, **70,** 582-594.
Mathews, W. H. and Mackay, J. R. (1960). Deformation of soils by glacier ice and the influence of pore pressures and permafrost. *Trans. R. Soc. Can.*, **54,** Ser. 3, Sect. 4, 27-36.
Mathews, W. H. and Mackay, J. R. (1964). Discussion of "Role of permafrost in ice-thrusting". *J. Geol.*, **72,** 378-380.
Mathews, W. H. and Mackay, J. R. (1965). Discussion of "Ice-pushed ridges, permafrost and drainage". *J. Geol.*, **73,** 896.
Moran, S. R. (1971). Glaciotectonic structures in drift. *In* Goldthwait, R. P., Ed., *Till: a symposium.* Ohio State University Press, 402 pp.
Nye, J. F. (1952). The mechanics of glacier flow. *J. Glaciology*, **2,** 82-93.
Potter, P. E. and Pettijohn, F. J. (1963). Paleocurrents and basin analysis. Springer-Verlag, Berlin, 296 pp.
Ramsay, J. G. (1967). Folding and fracturing of rocks. McGraw-Hill, New York, 568 pp.
Ramsay, J. G. and Graham, R. H. (1970). Strain variation in shear belts. *Can. J. Earth Sci.*, **7,** 786-813.
Rusnak, G. A. (1957). The orientation of sand grains under conditions of "unidirectional" fluid flow. 1. Theory and experiment. *J. Geol.*, **65,** 384-409.
Rust, I. C. (1967). *On the sedimentation of the Table Mountain Group in the western Cape Province.* D.Sc. thesis (unpubl.), Univ. Stellenbosch, 110 pp.
Rutten, M. G. (1960). Ice-pushed ridges, permafrost and drainage. *Am. J. Sci.*, **258,** 293-297.
Rutten, M. G. (1965). Discussion of "Ice-pushed ridges, permafrost and drainage". *J. Geol.*, **73,** 895-896.
Slater, G. (1926). Glacial tectonics as reflected in disturbed drift deposits. *Proc. geol. Ass.*, **37,** 392-400.
Slater, G. (1927a). Part I. The structure of the disturbed deposits in the lower part of the Gipping Valley near Ipswich. *Proc. geol. Ass.*, **38,** 157-182.
Slater, G. (1927b). Part II. The structure of the disturbed deposits of the Hadleigh Road area, Ipswich. *Proc. geol. Ass.*, **38,** 183-216.
Slater, G. (1927c). The structure of the Mud Buttes and Tit Hills in Alberta. *Bull. geol. Soc. Am.*, **38,** 721-730.
Spencer, E. W. (1969). Introduction to the structure of the earth. McGraw-Hill, New York, 597 pp.
Sugden, D. E. and John, B. S. (1976). Glaciers and landscape. Edward Arnold, London, 376 pp.
Theron, J. N. and Blignault, H. J. (1973). A model for the sedimentation of the Dwyka glacials in the southwestern Cape, 347-356. *In* Campbell, K. S. W., Ed., *Gondwana Geology.* Austr. National University Press, Canberra, 705 pp.
Turner, F. J. and Weiss, L. E. (1963). Structural analysis of metamorphic tectonites. McGraw-Hill, New York, 545 pp.
Viete, G. (1960). Zur Entstehung der glazigenen Lagerungs-störungen unter besonderer Berücksichtigung der Flözdeformationen im mitteldeutschen Raum. Freiberger Forschungshefte c78. Akademie Verlag, Berlin.
Visser, J. N. J. (1962). *Die voorkoms en oorsprong van die tillietband in die Serie Tafelberg.* M.Sc. thesis (unpubl.), Univ. Orange Free State.
Visser, J. N. J. (1965). Gletservloer in die Pakhuisberge, distrik Clanwilliam. *Ann. geol. Surv.*, Dept. Mines, **4,** 43-48.
Whitten, E. H. T. (1966). Structural geology of folded rocks. Rand McNally, Chicago, 678 pp.
Williams, E. (1960). Intra-stratal flow and convolute folding. *Geol. Mag.*, **97,** 208-214.

MAP 1

GEOLOGICAL DETAIL MAP, DE TRAP

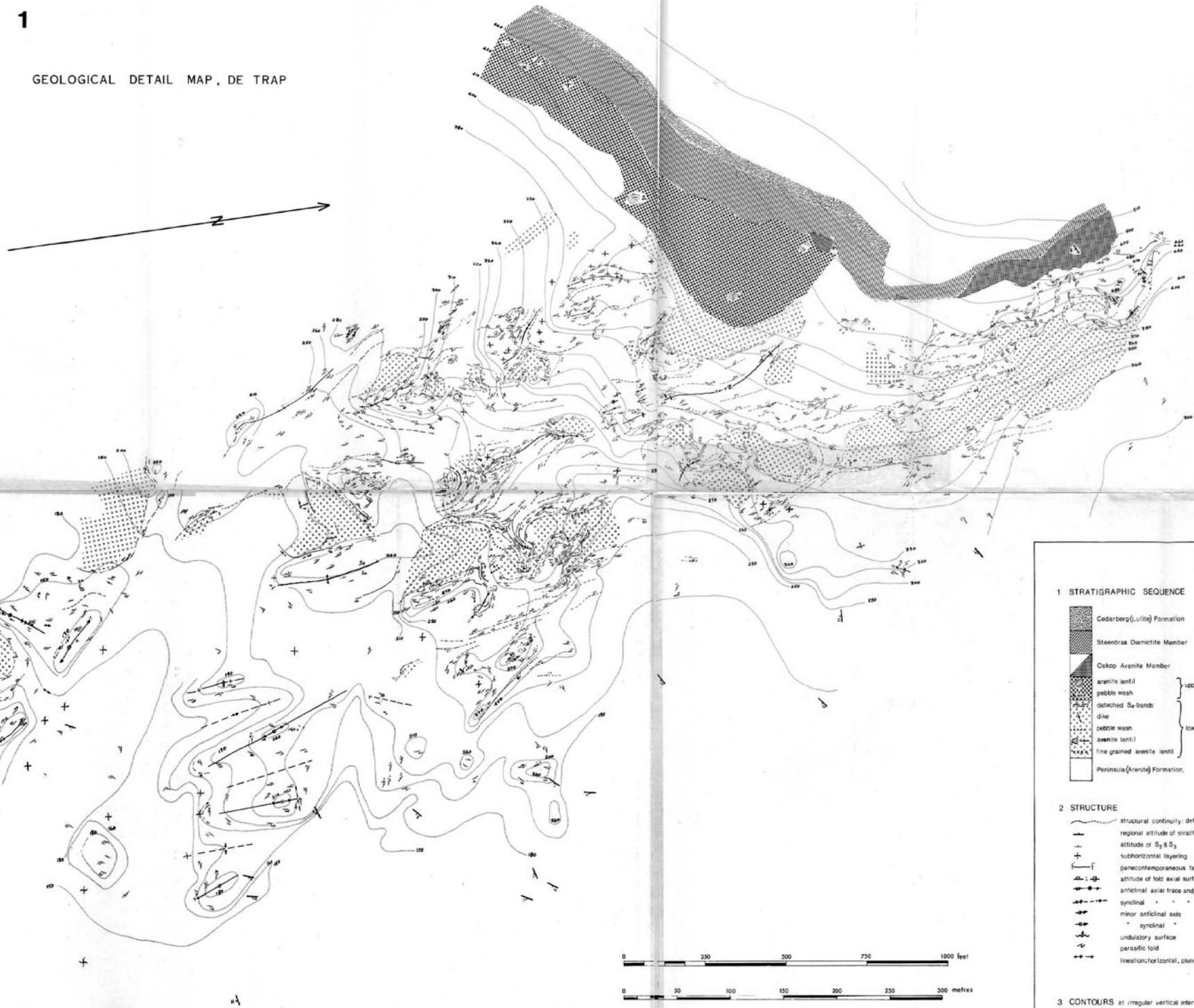

LEGEND

1 STRATIGRAPHIC SEQUENCE

- Cedarberg (Lutite) Formation
- Steenbras Diamictite Member
- Oskop Arenite Member
- Sneeukop Diamictite Member (upper): arenite lentil; pebble wash
- Sneeukop Diamictite Member (lower): detached S_4-bands; dike; pebble wash; arenite lentil; fine grained arenite lentil
- Pakhuis Formation
- Peninsula (Arenite) Formation

2 STRUCTURE

- structural continuity: definite - approximate - conjectural
- regional attitude of stratification (S_2)
- attitude of S_2 & S_3
- subhorizontal layering
- pericontemporaneous fault
- attitude of fold axial surface; recumbent
- anticlinal axial trace and/or axis; horizontal, culmination, plunge
- synclinal " " " " ; " " , plunge
- minor anticlinal axis
- " synclinal "
- undulatory surface
- parasitic fold
- lineation; horizontal, plunging

3 CONTOURS at irregular vertical intervals (in feet)

MAP 2

GEOLOGICAL INTERPRETATION MAP, DE TRAP